SOLAR MICROWAVE BURSTS – A REVIEW

MUKUL R. KUNDU and LOUKAS VLAHOS

Astronomy Program, Department of Physics and Astronomy, University of Maryland, College Park, MD 20742, U.S.A.

(Received 11 January, 1982)

Abstract. We review the observational and theoretical results on the physics of microwave bursts that occur in the solar atmosphere. We particularly emphasize the advances made in burst physics over the last few years with the great improvement in spatial and time resolution especially with instruments like the NRAO three element interferometer, Westerbork Synthesis Radio Telescope and more recently the Very Large Array (VLA).

We review the observations on pre-flare build-up of an active region at centimeter wavelengths. In particular we discuss the observations that in addition to the active region undergoing brightness and polarization changes on time scales of the order of an hour before a flare, there can be a change of the sense of polarization of a component of the relevant active region situated at the same location as the flare, implying the emergence of a flux of reverse polarity at coronal levels. The intensity distribution of cm-λ bursts is similar to that of soft X-ray and hard X-ray bursts. Indeed, it appears that the flaring behavior of the Sun at cm wavelengths is similar to that of some other cosmic transients such as flare stars and X-ray bursters.

We discuss three distinct phases in the evolution of cm bursts, namely, impulsive phase, post-burst phase, and gradual rise and fall. The radiation mechanism for the impulsive phase of the microwave burst is gyrosynchrotron emission from mildly relativistic electrons that are accelerated near the energy release site and spiral in the strong magnetic field in the low corona. The details of the velocity distribution function of the energetic electrons and its time evolution are not known. We review the spectral characteristics for two kinds of velocity distribution, e.g., Maxwellian and Maxwellian with a power law tail for the energetic electrons. In the post-burst phase the energetic electrons are gradually thermalized. The thermal plasma released in the energy release region as well as the expanded parts of the overheated upper chromosphere may alter the emission mechanism. Thus, in the post-burst phase, depending on the average density and temperature of the thermal plasma, the emission mechanism may change from gyrosynchrotron to collisional bremsstrahlung from a thermal plasma. The gradual rise and fall (GFR) burst represents the heating of a flare plasma to temperatures of the order of 10^6 K, in association with a flare or an X-ray transient following a filament disruption.

We discuss the flux density spectra of centimeter bursts. The great majority of the bursts have a single spectral maximum, commonly around 6 cm-λ. The *U*-shaped signature sometimes found in cm-dcm burst spectrum of large bursts is believed to a be a reflection of only the fact that there are two different sources of burst radiation, one for cm-λ and the other for dcm-λ, with different electron energy distributions and different magnetic fields.

Observations of fine structures with temporal resolutionof 10–100 ms in the intensity profiles of cm-λ bursts are described. The existence of such fine time structures imply brightness temperatures in burst sources of order 10^{15} K; their interpretation in terms of gyrosynchrotron measuring or the coherent interaction of upper hybrid waves excited by percipitating electron beams in a flaring loop is discussed.

High spatial resolution observations (a few seconds of arc to $\sim 1''$ arc) are discussed, with special reference to the one- and two-dimensional maps of cm burst sources. The dominance of one sense of circular polarization in some weak 6 cm bursts and its interpretation in terms of energetic electrons confined in an asymmetric magnetic loop is discussed. Two-dimensional snapshot maps obtained with the VLA show that multi-peak impulsive 6 cm burst phase radiation originates from several arcades of loops and that the burst source often occupies a substantial portion of the flaring loop, and is not confined strictly to the top of the loop. This phenomenon is interpreted in terms of the trapping of energetic electrons due to anomalous doppler resonance instability and the characteristic scale length of the magnetic field variation along the loop. The VLA observations also indicate that the onset of the impulsive phase of a 6 cm burst can be associated with the appearance of a new system of loops. The presence of two loop systems with opposite polarities or a

Space Science Reviews **32** (1982) 405–462. 0038–6308/82/0324–0405$08.70.

quadrupole field configuration is reminiscent of flare models in which a current sheet develops in the interface between two closed loops.

We provide an extensive review of the emission and absorption processes in thermal and non-thermal velocity distributions. Unlike the thermal plasma where absorption and emission are inter-related through Kirchoff's law, the radiation emitted from a small population of non-thermal electrons can be reabsorbed from the same electrons (self-absorption) or from the background (thermal) electrons through gyro-resonance absorption, and free-free absorption. We also suggest that the non-thermal electrons can be unstable and these instabilities can be the source of very high brightness temperature, fine structure (~ 10 ms) pulsations.

Finally in the last part of this review we present several microwave burst models – the magnetic trap model, the two-component model, thermal model and the flaring loop model and give a critical discussion of the strength and weakness of these models.

Contents

1. Introduction

The radio bursts are observed at all wavelengths from millimeter and centimeter wavelengths down to meter and decameter wavelengths, and therefore they originate from all levels of the solar atmosphere – from the chromosphere to the outer corona. The study of centimeter wave bursts is important because they occur in the same region of the sun's atmosphere where the flare explosion takes place. Consequently, the centimeter burst radiation provides information on the region of energy release and acceleration of electrons to relativistic or mildly relativistic energies. The centimeter-wave bursts are simple: they are characterized by a rapid rise in intensity and a slower decline. The burst radiation is in general smooth, usually free of details in time and frequency and is a partially polarized broadband continuum. It starts almost immediately after an associated Hα flare and originates from a source of small angular size ($< 1'$ arc). The smooth continuum emission of centimeter-wave bursts has been accounted for by gyrosynchrotron raiation from fast electrons accelerated during flares. In this review, we shall first describe the observational characteristics of centimeter-wave bursts and then examine the different theories that have been proposed to explain their origin.

The properties of centimeter wave bursts and their interpretations were summarized by Kundu (1963, 1965) several years ago. However, at that time, the spatial resolution available was only $\sim 1'$ arc. Even with this resolution the presence of small scale structures in cm-λ bursts sources was established by Kundu (1959) who obtained estimates of burst sizes between $1'$ and $3'5$ with a 2-element interferometer. Since that time there have been a number of observations with fan beam interferometers, primarily from Toyokawa (e.g., Enome *et al.*, 1969) with spatial resolution as good as $24''$ and more recently from Stanford (e.g., Felli *et al.*, 1975) with $16''$ resolution, which have revealed smaller scale structures and more complexity in the burst regions. Significantly better resolution, of up to $1''$ arc has been achieved with the NRAO interferometer, the Westerbork Synthesis Radio Telescope, and the Very Large Array; observations with such spatial resolution have revealed structures of only a few arc seconds (see e.g., Kundu *et al.*, 1974a; Kundu and Alissandrakis, 1975; Alissandrakis and Kundu, 1978; Marsh *et al.*, 1979; Kundu *et al.*, 1977, 1981a, 1982b). At the same time soft X-ray observations, particularly from Skylab, with resolution better than $5''$ (e.g., Kahler *et al.*, 1975; Vorpahl *et al.*, 1975) have provided new information about the flare phenomenon; these observations are of particular relevance to the cm-λ observations due to the close association of soft X-ray and cm-λ burst sources (Kundu *et al.*, 1976; Pallavicini and Vaiana, 1976). These high spatial resolution observations are particularly important for a proper understanding of the generating mechanism of cm-λ bursts, acceleration of electrons and the origin of solar flares. Earlier attempts at theoretical studies of cm-λ burst emission were based mainly upon low resolution ($\gtrsim 1'$ arc) data. With the avail-

ability of resolution of the order of 1″ arc and time resolution of ~ 10 ms, there has been renewed activity on the theoretical side. In this review we propose to give an up-to-date account of cm-λ burst observations including high spatial and time resolution data, and the recent theoretical models that have been proposed. A relatively recent review of the observational aspects of cm-λ bursts has been provided by Kundu (1980).

2. Observations

2.1. Flare precursor

For understanding fully the flare process one must know the background environment in which the flare occurs, namely the active region. During active periods of the Sun, there are always present on the solar disk sources of slowly varying radiation which persist from several days to several solar rotations. Interferometric observations at 3 cm wavelength with an angular resolution of ~ 1′5 arc made more than 20 years ago (Kundu, 1959) indicated that these sources are usually of large diameter ($\gtrsim 3'$ arc); however, at times of high solar activity, there often occur at 3 cm wavelength intense sources of very small diameter ($< 1'$ arc). These sources are strongly polarized, and they last for only several days – presumably associated with the peak of evolution of the sunspot group. The polarized intense source is a result of the sunspot magnetic field and is produced by gyroresonance emission at harmonics of the gyrofrequency, whereas the unpolarized diffuse sources associated with plage regions is due to bremsstrahlung in the condensations of higher density than in the surrounding regions. The flare-associated bursts originate near these intense sources, and the probability of occurrence of bursts increases with the increasing intensity of these narrow bright regions (Kundu, 1959). Of particular importance is the fact that flares associated with type IV bursts tend to occur more frequently in the intense regions of small diameter than in the diffuse regions of low intensity. This behaviour of the active regions prior to the onset of flares has also been observed on spatial scales of a few arc seconds (Kundu *et al.*, 1974b; Lang, 1974). Indeed, using the Owens Valley interferometer at 2.8 cm-λ with a resolution of 7″ arc, Lang (1974) observed circular polarization in the visibility function of up to 100% in the active region core (see Figure 1). Lang (1977) also claimed that dramatic changes (of up to 80%) in the circular polarization of the visibility function (within spatial scales of ~ 5″ arc) occurred approximately one hour before the flare onset. By contrast, according to Lang, no substantial variations in polarization were observed over a quiescent period of forty hours. Although Lang had data for only two cases, he speculated that the pre-flare polarization changes might be related to emerging magnetic fields triggering flares.

There are two processes involved in the occurrence of a flare; one is the gradual storage of magnetic energy, and the other is a trigger action to release the stored energy. Observations of an active region prior to the onset of a flare are of obvious importance to our understanding of the flare build-up process. At short centimeter wavelengths (2–6 cm), one observes this flare build-up in the form of increased intensity and increased polarization of the active region, both of which suggest that the magnetic field increases

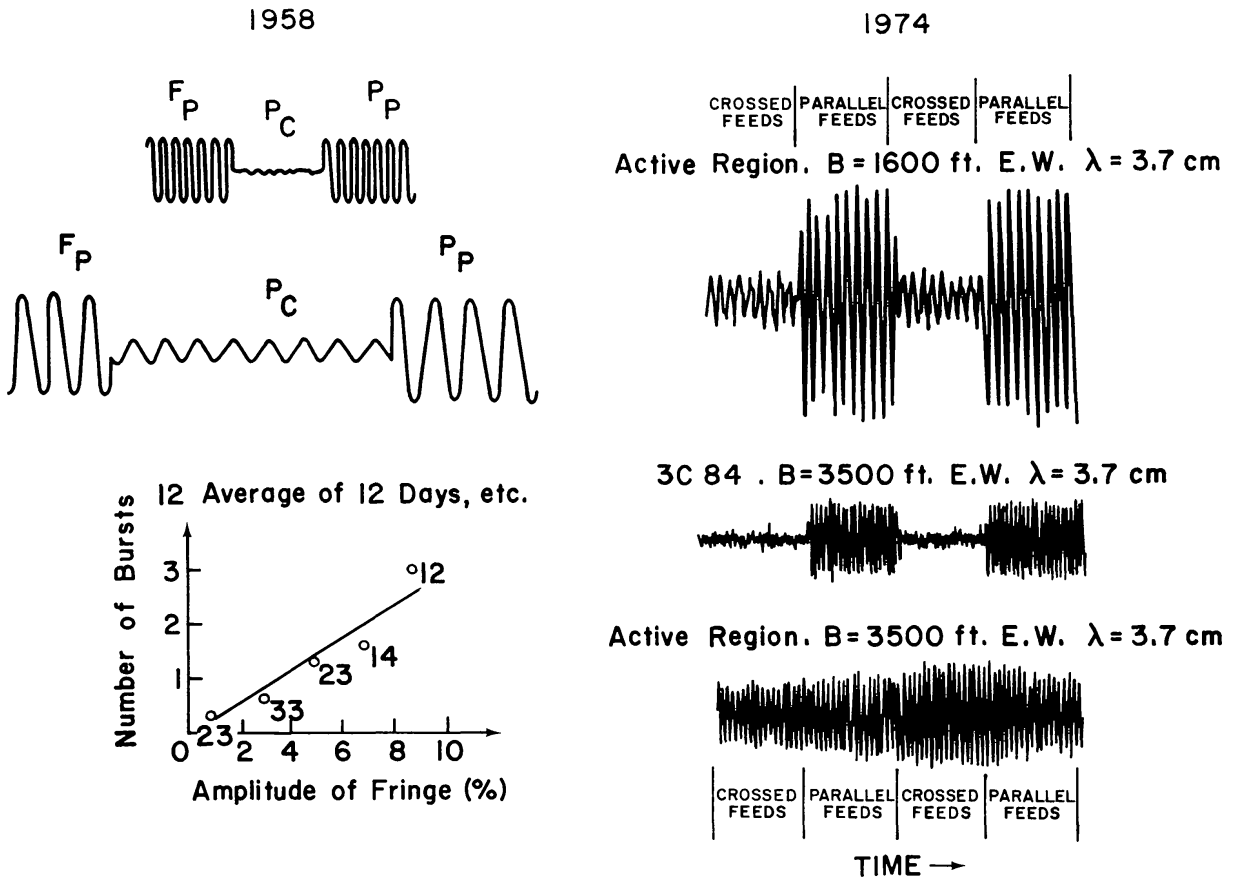

Fig. 1. *Top left:* 3 cm solar interferometric observations with crossed and parallel feeds. *Lower left:* number of 3 cm-λ bursts as a function of the amplitude of fringes observed at mid-day (H.A. $\simeq 0°$) expressed as a percentage of the quiet Sun emission (after Kundu, 1959). *Right:* 3.7 cm interferometric observations with crossed and parallel feeds (after Lang, 1974).

or becomes more ordered prior to the occurrence of the flare. Skylab X-ray observations have also provided evidence for flare build-up in the form of preheating of X-ray kernels. It seems, however, that the flaring kernel is not necessarily the one that undergoes preheating. It should be remembered that soft X-ray preheating refers to 2–3 min before the onset of the main flare, while the radio observations refer to one to two hours before the onset. Since the radio observations provide information on the magnetic field, it is of extreme importance to study the flare build-up at centimeter wavelengths with an angular resolution of 1″ arc or less. With the VLA it was possible to produce two-dimensional synthesized maps over short periods before the start of a flare. In the case of a hard X-ray associated impulsive centimeter burst observed on June 25, 1980, Kundu *et al.* (1982b) had good active region data for about one hour prior to the flare start. They produced several 15-min synthesized maps in total intensity (I) and polarization (V). Figure 2, shows the central 1′1 × 1′6 region of 15 min synthesis maps over the period 14 : 45–15 : 45 UT. As can be seen from these figures, the region is very complex, consisting of numerous components many of which are bipolar. These oppositely polarized components could be the footpoints of magnetic loops. Near the center of the field of view, the component regions marked A, B, C (which appear in all the pre-flare maps) seem to be arranged in clearly separated regions of opposite polarity. The

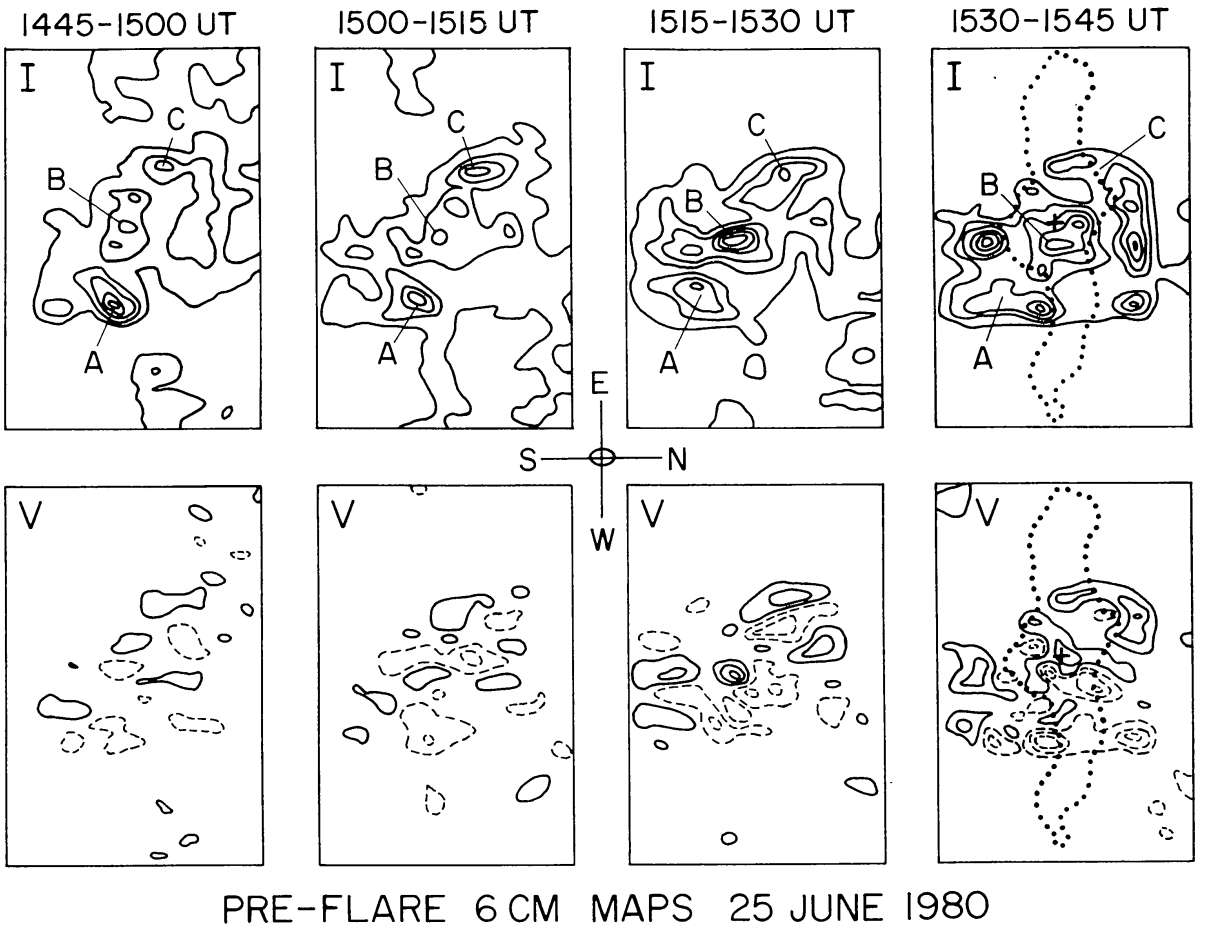

Fig. 2. Central 1′1 × 1′6 regions of Pre-flare (15^m) maps of I and V. 15 : 00–15 : 45 UT, 25 June, 1980. The beam size is 4″ × 6″ arc. The first contour is 1 × 10^6 K and the contour interval is 2 × 10^6 K. Note the reversal of polarity in component '*B*' in the last map, close to the subsequent burst peak (marked by a +). The dotted outline shows the extent of the burst source in the impulsive phase, 15 : 51–16 : 00 UT (after Kundu *et al.*, 1982b).

components have brightness temperatures of 6–9 × 10^6 K during the hour before the flare. Similar high brightness temperatures $\gtrsim 10 \times 10^6$ K were also observed in the pre-flare region of 14 May 1980 event (see Section 2.8(ii)). The burst of 25 June, 1980 starting at 15 : 50 UT (see Section 2.8(i)) was located close to the neutral line of these oppositely polarized regions near *B*. The burst maximum is identified with a '+' and the burst extent averaged over the period 15 : 51–16 : 00 UT is shown by the dotted contour in the last map (Kundu, 1981; Kundu *et al.*, 1982b).

As one can see from these maps, there was a definite trend for the active region undergoing brightness and polarization changes. The central component *B* intensified at 15 : 15–15 : 30 UT and increased in polarization slightly. In the last map (15 : 30–15 : 45) several new components appeared with polarizations of 40–80%. However, the most remarkable feature is the change of the sense of polarization of component *B* (see Figure 2); also the component on the northern side of *B* greatly increased in polarized intensity, with polarization of 80–90%. This might imply the emergence of a flux of reverse polarity at coronal levels. (The photospheric magnetograms show little or no change.) Consequently, we feel that we may be dealing with a

pre-flare activity similar to the one considered in the flare model of Heyvaerts *et al.* (1977). It is not entirely clear how the reverse polarity could occur at coronal levels without any corresponding signature in the photosphere. We believe that this may be caused by the emergence of a new flux tube in the corona, and subsequent twisting increases its magnetic field so that it becomes equal to or higher than that corresponding to the third harmonic of the gyrofrequency (600 G at 6 cm-λ); at the same time there must be some heating of the loop. Alternately one can conceive of a previously existing loop of opposite polarity which was not observable at 6 cm due to its weak magnetic fields; it is possible that a sudden onset of currents in the loop builds its field strength in the corona to values of the order of 600 G in order for it to be observable at 6 cm-λ.

2.2. Intensity distribution of cm-λ bursts

The transition from the precursor stage to the 'actual' burst must be a matter of definition, since the burst intensity varies from a value barely discernible above receiver noise to thousands of solar flux units. To understand the physics of energy build-up and release in flares it may be useful to study the intensity distribution of flares. Such studies have been carried out in terms of plots of number histograms of observed events against integral of peak fluxes of the events. Such plots presented for centimeter bursts (Kundu, 1965), for soft X-ray bursts (Drake, 1971) and for hard X-ray events (Datlowe *et al.*, 1974) show that in each case a power-law fit for the number of events per intensity interval provides a good fit. The intensity distribution of the centimeter-wavelength bursts can be represented as shown in Figure 3a and by a curve which fits the equation, $F(I) = (\Delta N/\Delta I)I^{-x}$, where $x = 1.5$ at 3 and 10 cm-λ. The term $F(I)$ is the frequency of occurrence of centimeter-wavelengths bursts of mean intensity I, and ΔN is the number of bursts in the intensity interval ΔI. This flaring behavior of cm-λ bursts is similar to the flaring frequency observed in soft X-rays (see Figure 3b); Drake (1971) found that the number histogram of solar soft X-ray burst occurrence when plotted against the total integrated flux $E_T = \int F \, dt$ for each event, can be fitted by a power-law with an exponent 1.44, similar to that found at cm-λ. Indeed, generalizing this flaring behavior for a variety of cosmic transient sources – the Sun, Flare Stars (such as UV Ceti, YZ CMi see Figure 3c) and X-ray bursters which span an energy release rate of more than 10 decades, Rosner and Vaiana (1978) showed that the frequency (ν) as a function of energy released (E) follows a similar power-law [($\nu(E) \propto E^{-x}$)] at large energies for all these sources. Rosner and Vaiana (1978) tried to interpret these distributions of the flare energy release process, as follows: they suggested that external forces supply energy to the pre-flare region at a rate proportional to the internal energy of the system. This suggestion is understandable in terms of Parker's (1977) theoretical arguments, that magnetic fields produced in the convecting Sun and other objects in the astrophysical universe are the cause of the activity observed in these objects. Strong magnetic fields imply vigorous photospheric fluid motions, which in turn preturb and twist the emerging magnetic fields. This is related to the intuitive suggestion of Rosner and Vaiana, if we identify the internal energy of the pre-flare region as the already emerged magnetic field and the external forces as the convective fluid motions. Assuming that Poisson statistics governed the flare

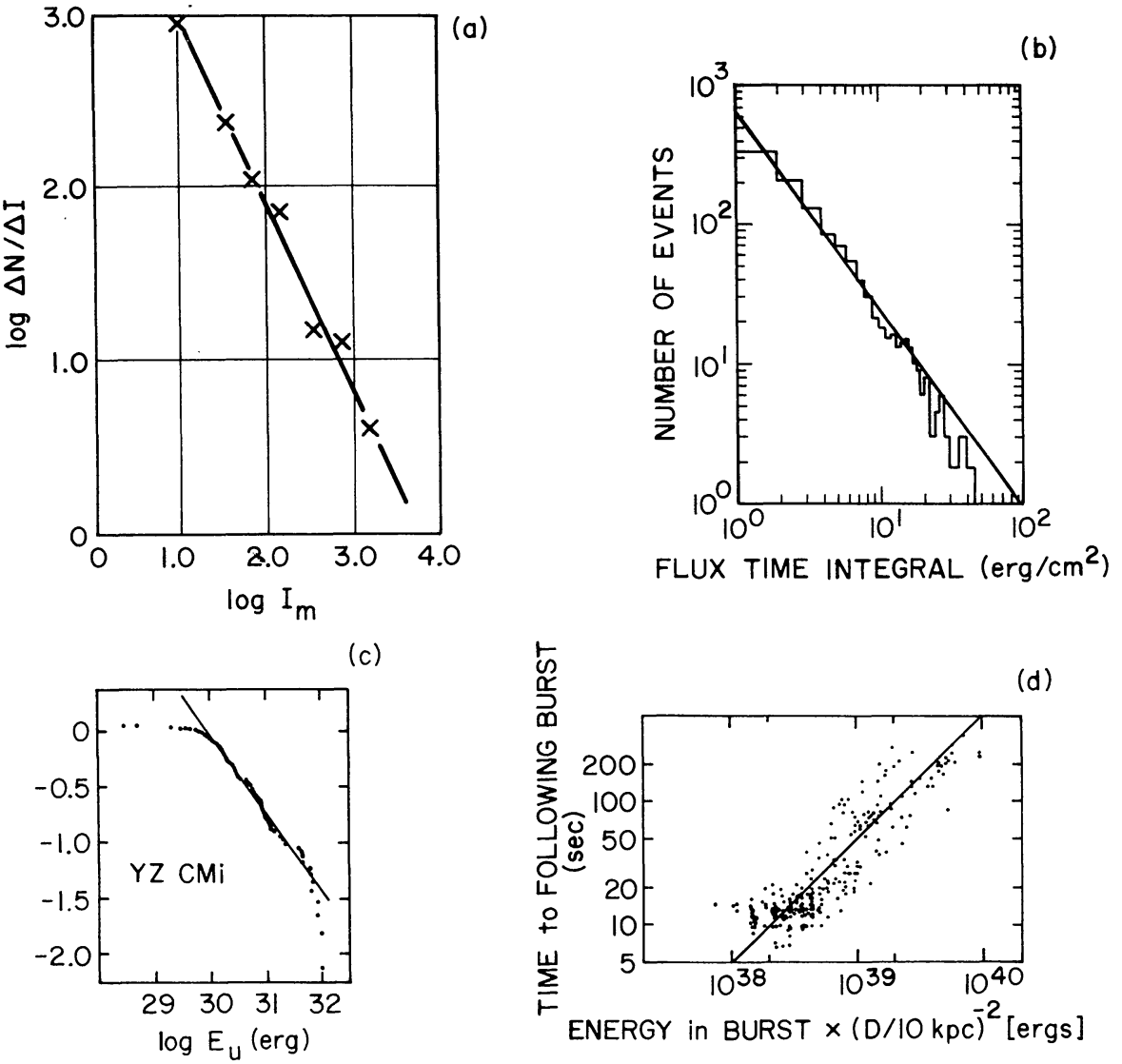

Fig. 3. (a) Plot of log $\Delta N/\Delta I$ as a function of log I where ΔI = intensity interval; ΔN = number of bursts in the interval ΔI. I = is the mean intensity and is presented in units of 10^{-22} Wm^{-2} (c/sec)$^{-1}$ (after Kundu, 1965). (b) Number Histogram of solar soft X-ray flare occurrence detected by Explorers 33 and 35 (Drake, 1971), plotted against the total integrated flux $\int F\,dt$ for each event. The power-law fit shown is due to Drake (1971) and is characterized by an exponant 1.44 ± 0.01. (c) Frequency histograms of optical flare occurrence from *YZ CM*$_i$ plotted against the total flare energy radiated in the U band pass for each flare (Lacy *et al.*, 1976). (d) Correlation diagram of the time interval between an X-ray burst from MXB 1730–335 and the next succeeding burst, and the X-ray energy in the first burst as published by Lewin *et al.* (1976). Also shown is a line indicating the expected behavior, if the energy in the first burst were linearly related to the time interval between succeeding bursts (after Rosner and Vaiana, 1978).

probability in time, Rosner and Vaiana derived a power-law distribution for flare energies with the exponent equal to the ratio between the mean flaring rate and the energy build-up rate. A logical consequence of this unified description of the flaring process for diverse cosmic transients, is that the total energy released by a given flare must be related to the elapsed time since the last preceding flare, because increasing the interflare duration permits greater energy storage within the flaring region (if the source is a single flaring region). An example was provided by the X-ray source MXB 1730–335, Figure 3d.

Similar behavior has been noticed in the case of solar flares, namely, largest radio burst occur during the decreasing or increasing phase of the solar activity cycle when there is more time available between bursts for energy to build-up (Kundu, 1980).

The centimeter-wavelength bursts tend to be more intense and more numerous during periods of maximum sunspot activity than during minimum (Kundu, 1965). During the maximum of solar activity cycle, the average number varies between zero during quiet periods and two or more per day during active periods. This behavior is quite understandable since during the period of maximum activity, the active regions are more numerous than during minimum and so there is a greater probability for magnetic reconnections. Indeed, using the general theoretical arguments developed by Parker (1977) again, we can qualitatively understand the above behavior as follows. The magnetic fields in the active regions are restless, continually manipulated by the convection zone and the photospheric fluid motions, the twisted components continually rise up through the surface into the apex of each re-entrant flux tube. The magnetic field lines try to reach equilibrium through reconnections, and in so doing heat the plasma and/or accelerate particles. The interaction of this hot plasma or the energetic electrons with the magnetic field appears at microwave bursts (gradual or impulsive). In that sense microwave bursts are the reflection of the continual activity taking place below the surface of the Sun.

2.3. Different phases in cm-λ burst evolution

The centimeter-wave bursts are characterized by their simplicity as compared with the complex nature of the meter-wave bursts. The bursts on centimeter waves in most cases have a simple rise to maximum (sometimes there may be more than one maximum) and a much slower decay.

Meter-wave bursts have been classified into a number of distinct spectral types – types I, II, III, IV, and V, based upon the nature of emission (continuum or otherwise) and the drift of certain specific emitting features from high to low frequencies. The cm-λ bursts are mostly continuum in nature – similar to type IV and V of meter-wave emission; occasionally fine structure bursts are superimposed on this continuum. Although the cm-λ burst is always continuum in nature, its properties, especially the spatial structure, polarization and brightness temperature change in course of the burst. Three physically significant phases in the burst emission were thus distinguished by Kundu (1959).

(i) *Impulsive Phase*

The impulsive phase is characterized by a rapid rise to a peak intensity and a subsequent decline. It is short in duration (1 to 5 min). About 60% of these bursts are found to be partially circularly polarized. The burst source has a diameter varying from 10″ to 1′ arc. The peak brightness temperatures range from 10^8 K to about 10^9 K. It has been proposed (see Section 4) that this phase is caused by gyrosynchrotron radiation from nonthermal energetic electrons released and accelerated during the flare.

(ii) *Post-Burst Phase*

It follows a simple impulsive burst or a group of simple bursts (in the case of a complex structure). It has a duration of approximately several minutes to an hour. The polarization of the burst in this phase gradually decreases from that of the impulsive phase preceding it and ultimately becomes zero. Usually its source appears to be a diffuse region of relatively large diameter ($> 1'$ arc). Its brightness temperature usually lies between 10^5 K and 10^7 K. This burst appears to represent the thermalization process of the energetic electrons responsible for the impulsive phase. The impulsive phase is almost always followed by the post-burst phase, although claims have been made (Crannell *et al.*, 1978) that occasionally impulsive phase occurs in isolation. Usually these bursts are short in duration and it is difficult to separate the post-burst from the impulsive phase.

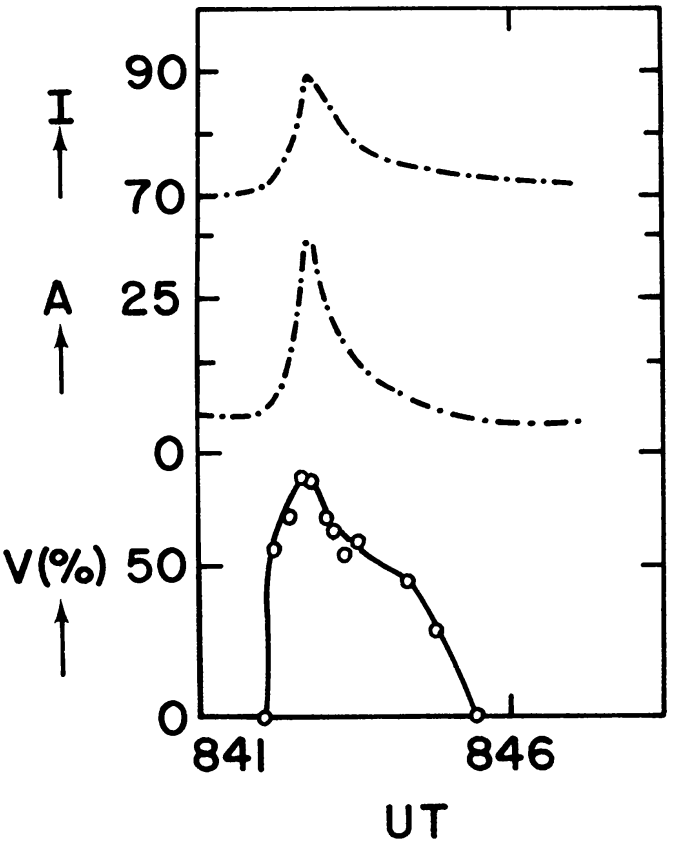

Fig. 4. Evolution of a simple burst on 3 cm-λ observed on November 16, 1957. I = total intensity, A = amplitude of fringes, V = visibility of fringes. The visibility curve is simple with only one maximum. Maximum visibility implies minimum size (after Kundu, 1959).

Even in these cases, the decay is slower than the rise, implying that there may, indeed, be a post-burst present. The evolution of burst size is such that for the impulsive phase the burst diameter is minimum around maximum intensity, implying that the emissive region (hot and dense plasma) is very localized around maximum intensity (Figure 4) and then gradually becomes more and more diffuse until its temperature and density become identical to those of the ambient medium (corona).

(iii) *Gradual Rise and Fall Burst*

It is characterized by a slow rise to maximum intensity and comparatively slower decline to the pre-burst level. Its duration is usually of the order of 10 min or longer. It is, in most cases, partially circularly polarized. Its source is a localized hot region of small diameter ($\leq 1'$ arc) with an equivalent temperature usually of the order of 10^6 K. This burst represents heating of the flare plasma. The 'GRF' usually occurs whenever a plasma is heated; it may occur even in the absence of a flare; for example, it occurs in association with X-ray transients that follow the disruption of filaments, without any accompanying chromospheric (Hα) flare emission (Figure 5). The X-ray transients represent a plasma heated to temperatures of 2–3 $\times$ 10^6 K.

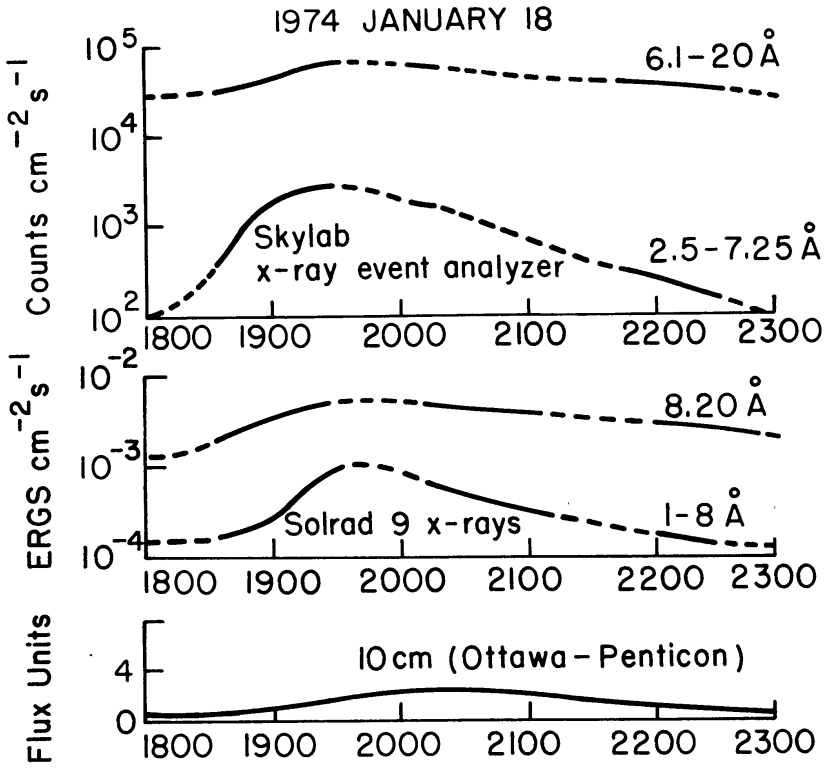

Fig. 5. The time history of the integrated solar flux in the soft X-ray and microwave-radio spectral bands illustrating the gradual-rise-and-fall (GRF) signature of this disappearing filament event. The traces shown are from the Skylab X-ray event analyzer 6.1–20 Å and 2.5–7.25 Å bands, the SOLRAD 8–20 Å and 1–8 Å bands, and the combined Ottawa-Penticton 10-cm radio emission. For each curve, dashes indicate intervals for which X-ray flux observations were not obtained, either because the respective satellite was in the Earth's shadow, or because Skylab was not configured for ATM observations. Note that the XREA fluxes are given in counts $cm^{-2}\,s^{-1}$ whereas the SOLRAD fluxes are given in erg $cm^{-2}\,s^{-1}$. Although each of these curves seems to reach its maximum sometime in the unobserved interval near 19 : 50 UT, the high-energy fluxes begin their decline sooner than the low-energy fluxes (after Sheeley *et al.*, 1975).

2.4. Flux Density Spectra

Single frequency observations show that the burst continuum sets in almost simultaneously on all frequencies in the centimeter wavelength range. For strong bursts, the continuum sometimes extends into the meter-wavelength region, but there the records show a great deal of fine structure, indicating a change in the emission mechanism

involved. In the centimeter wavelength region the intensity of a burst usually increases with frequency, following the relation $S \propto f^2$ up to $f = 5$ GHz; but there are also cases where the increase occurs more slowly. This part of the spectrum is followed by another, namely the post-burst phase where the intensity is almost independent of frequency. Sometimes, part of the spectrum also displays maxima in the region of rising intensity, and occasionally maxima are superimposed on the region of constant intensity. The maxima are broad; their intensity may rise to 5 times that of the adjoining continuum of equal energy.

Statistical peak flux-density spectra of centimeter bursts show that a great majority have a single spectral maximum, lying between 11 and 2 cm wavelengths. Most commonly the spectrum peaks at a wavelength around 6 cm. For gradual rise-and-fall bursts considered to be of thermal origin, Guidice and Castelli (1975) found that less than 20% had thermal spectra. It is possible that in the other cases, an additional nonthermal component coexisted with the thermal source, as has indeed been found from high spatial resolution observations (Kundu *et al.*, 1974a). Guidice and Castelli studied the relationship between the burst spectral maximum (f_{max}) and the photospheric magnetic field strength of the region associated with the burst. They found that there was a tendency for higher correlation at higher f_{max} with stronger magnetic fields. For bursts with cm components > 50 sfu it was found that statistically the low frequency cutoff f_{cut} was well correlated with f_{max}, with higher correlation for intensity 50–500 sfu bursts than for intensity > 500 sfu. For bursts of intensity 50–500 sfu a good fit to the relation $f_{max} = A f_{cut}$ was found with $A = 3.4$. When the peak flux density is plotted as a function

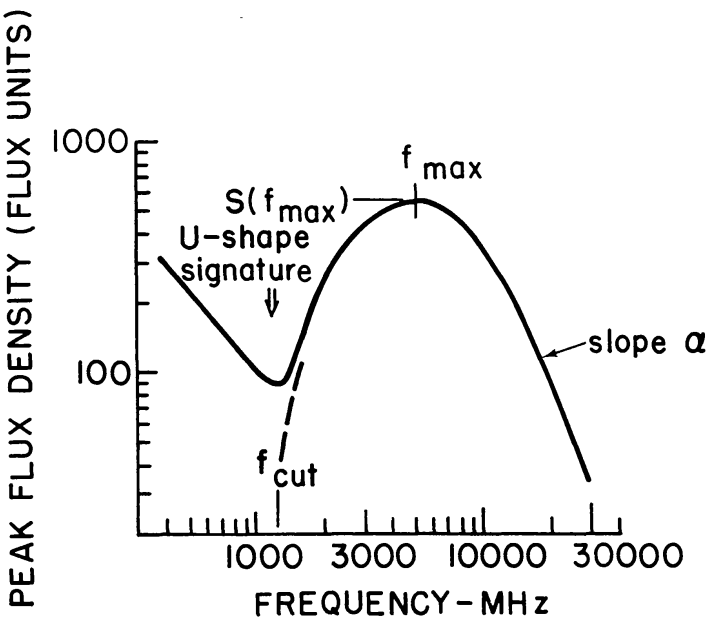

Fig. 6. Idealized peak-flux-density spectrum of a radio burst (representative of actual burst spectra) used for burst classification, emission-region parameter estimation, and signature detection (after Guidice and Castelli, 1975).

of frequency over the range 245 MHz–35 000 MHz, sometimes the bursts, especially the large ones show a U-shaped signature in the composite spectrum: the peak flux decreases from 245 MHz toward 1000 MHz, and then it increases again reaching a maximum around 5000 MHz, decreasing thereafter (Figure 6). We believe the U-shaped signature in the cm-dcm burst spectrum is a reflection of only the fact that there are two different sources of burst radiation – one for cm-λ and the other for dcm-λ. The two sources must have different electron energy distributions and different magnetic fields, with the result that their emission peaks occur at two different frequencies. As will be shown later (Section 3), the slope (α) on the high-frequency side of the centimeter component is related to the slope of the energy spectrum of the electrons responsible for the gyro-synchrotron emission observed in the centimeter range ($\alpha = (\gamma - 1)/2$). The cutoff frequency (f_{cut}) may be related to the electron density of the emitting region. Assuming that $f_{\text{cut}} \sim f_p$ and $f_{\max} \sim 4f_H$ the relation $f_{\max} \approx Af_{\text{cut}}$ gives a simple relation between the magnetic field and the density, namely $10^{-4} N_e \simeq B^2$ which implies that $\beta = (N_e kT_e)/(B^2/8\pi) \simeq 10^{-3}$, one order of magnitude higher than the result reported recently for a non-flaring loop by Kundu *et al.* (1979b).

Further, it appears that on a statistical basis, the peak frequency increases with the increasing flux density of the burst with a single maximum, according to the relation $S_{\max} \propto f_{\max}^2$ (Fürst, 1971). This simple relationship between the maximum intensity and frequency can be easily understood as follows: since $S_{\max}(\mathbf{E}, \mathbf{B})$ is a function of the average electron energy **E**, and magnetic field **B** in the microwave source and $\mathbf{E} \propto f'(B^2/8\pi)$ where f' is the fraction of the magnetic field that is transformed into electron energy, we can easily see that $S_{\max} \sim B^{\delta}$. At the same time $f_{\max} \sim 4f_{II} \propto B$, which implies that $\delta \simeq 2$. In other words, on the average, the flux density and the frequency during maximum are functions of the magnetic field alone. If we now interpret the statistical result of Castelli and Guidice, namely, that the microwave burst spectrum shows a peak around 5 GHz or 6 cm wavelength, we have to accept that the average magnetic field in the low coronal flaring loops is $\simeq 500$ G. This result is consistent with Stenflo's (1976) observation that the magnetic fields at the photospheric level, is concentrated in small tubes, with average field strength of ~ 2000 G in the photosphere.

The evolution of the cm-λ burst spectrum does not appear to be unique. In some cases, at the start of the event, the spectrum has a peak around 10 cm; with increasing time the peak shifts to longer wavelengths, and ultimately in the post-burst phase the spectrum becomes rather flat, resembling a thermal spectrum. In other cases, the frequency drift of the spectrum is comparatively small; this is a rather common characteristic of microwave bursts. It means that the time variation of the optical thickness which is proportional to the number density of energetic electrons is small during the burst. This would imply, according to Takakura (1973), that the region progressively moves from one place to another. Such a movement leaves the accelerated electrons behind during the increasing phase of the burst. Thereafter, the energetic electrons trapped in the magnetic tubes decay due to collisions and/or escape into the chromosphere. These implications will be discussed in detail in Section 4.

2.5. Polarization

In general, the polarization of strong bursts is circular and is much stronger (about 60 to 70%) at 1000 and 2000 MHz than at higher frequencies, where it is only of the order of 20 to 30%. Also, the sense of polarization changes in the decimeter wavelength region, usually somewhere between 2000 and 3750 MHz, indicating that the decimeter wavelength radiation is circularly polarized in the ordinary sense as compared to the extraordinary sense of polarization at higher frequencies (Tanaka, 1961; Tanaka and Kakinuma, 1962). It should be noted that the slowly varying component from the active region in which the burst occurs usually has an extraordinary sense of polarization. The ordinary mode of polarization of dcm bursts may be a genuine property of the source, as for example if the dcm continuum source is associated with the following spot of a bipolar region, in contrast to the cm source being associated with the leading spot (Takakura, 1962). It is also possible to explain it as a propagation effect caused by magneto-ionic mode coupling in a quasi-transverse region (Cohen, 1961) or by invoking differential absorption of the ordinary and extraordinary mode of gyrosynchrotron radiation near the gyrofrequency of ambient thermal electrons (Takakura, 1962).

2.6. Time structure

(i) *Time Structure with* ~ 1 s *Resolution*

It has been known (e.g., Kundu, 1965) for a long time that some centimeter wave bursts show fine structures in their intensity profiles and dynamic spectra. These fine structures are usually superposed on a continuum; examples of such fine structures can be seen in dynamic spectra in the range 2–4 GHz obtained with 1 s time resolution (see e.g., Kundu and Haddock, 1961). These structures resemble the fast drift bursts at meter wavelengths; both the continuum and fine-structure bursts may be associated with a group of meter-wave type III bursts. On single frequency records the fine-structure bursts appear as spikes superposed on a smooth continuum of much longer duration. The burst elements are of very short duration of the order of a fraction of a second, and they drift in both senses (forward and reverse) in the solar atmosphere. High spatial resolution observations of such fine structure bursts were recently made by Kattenberg (1981) with 0.1 s time resolution, and 3″ arc resolution at 6 cm using the WSRT. Kattenberg analyzed ten (rather weak) bursts and found that the 'spikes' and the 'continuum' often originated in different locations. He also showed that the spikes were randomly or weakly polarized in contrast to the continuum which was circularly polarized up to 40%.

Such fine structure bursts are much more common at decimeter wavelengths, 30 cm and longer. At these wavelengths they have been referred to as 'Generalized Fast-Drift' bursts, and they include bursts such as 'intermediate-drift', 'reverse drift', 'zebra bursts', 'spray bursts', etc. Descriptions of the properties of such bursts and their interpretations have been provided by Young *et al.* (1961), Kundu and Spencer (1963), Rosenberg (1971), and Kuijpers (1974). In this review we shall not deal with individual fine structure bursts. However, we shall first discuss the correlated time structures in cm-λ, hard X-ray

and EUV bursts; then we shall discuss the observations made recently by Slottje (1978) at 11 cm-λ with $\sim$ 10 ms time resolution because of the importance these observations play in the generating mechanisms of such bursts.

Parks and Winckler (1966) observed correlated 16-s periodic bursts during the impulsive phase of a flare in hard X-rays, microwaves and EUV (Figure 7). As we know, the hard X-rays and microwave impulsive events are generally well-correlated (Kundu, 1961). It appears that even the rapid periodic fluctuations are extensively correlated in microwaves and hard X-rays. Excellent correlation was also observed between X-rays and EUV radiation. The hard X-rays correlated best with the radio burst at 1.6 cm (Figure 7). The explosive phase was observed in Hα around 18 : 14 UT, the time of onset of the hard X-ray and impulsive microwave bursts (Janssens and White, 1970). The development of the flare area and the Hα line width resembled best the time profile of soft X-rays in the 2–12 Å. The periodic structures were predominantly a phenomenon of high energy electrons, $E > 80$ keV. Since the periodic X-ray structures were correlated

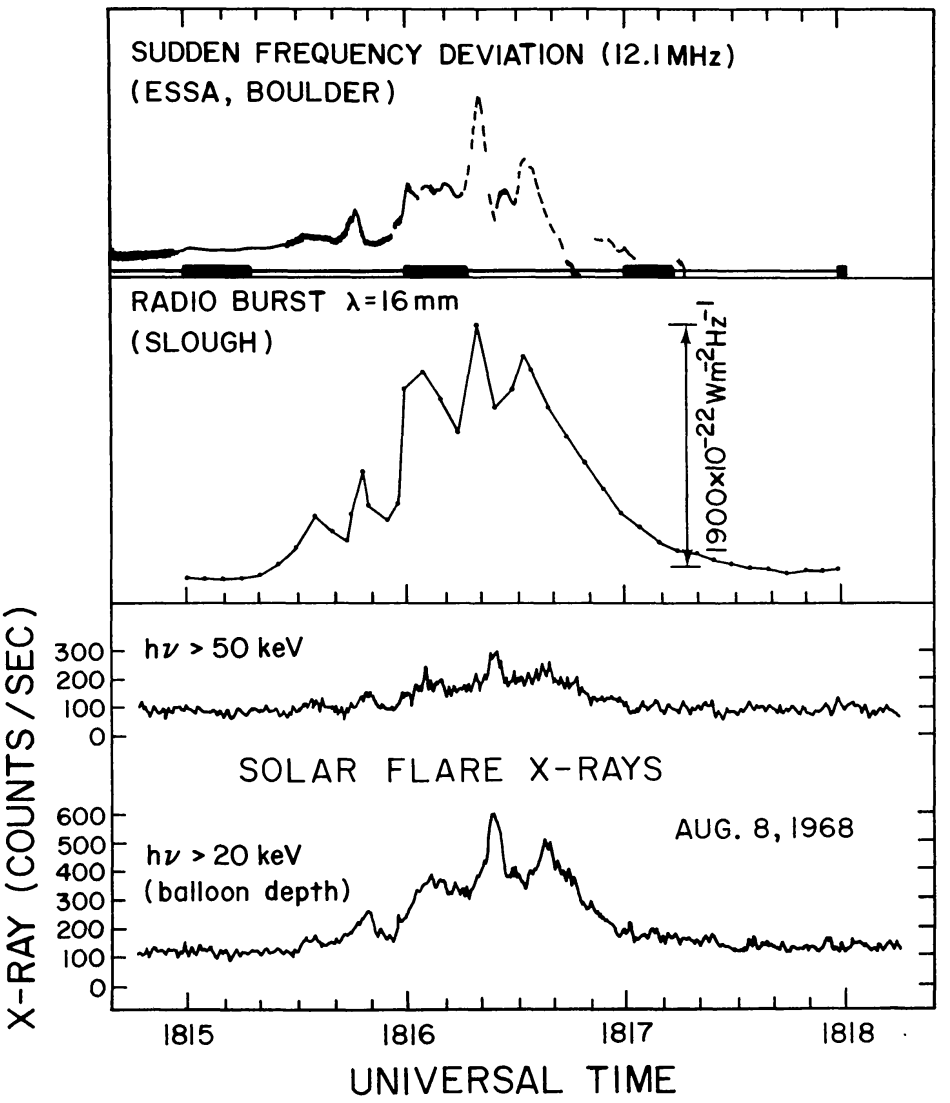

Fig. 7. The correlated periodic events in EUV, 1.6 cm radio waves and the hard solar X-rays (after Parks and Winkler, 1966).

well in microwave and EUV frequencies, a plausible conclusion was that these three types of radiation have a common energy source. This is consistent with the conclusion of de Jager and Kundu (1963) that the energetic electrons responsible for microwave and hard X-ray bursts must have a common source.

Similar periodic or quasi-periodic structures in hard X-ray bursts have been reported by Frost (1969). These hard X-ray burst observations prompted high sensitivity and high time resolution (< 1 s) observations of microwave bursts by several groups (e.g., Janssens *et al.*, 1973; Kaufman, 1968). Janssens *et al.* demonstrated the existence of

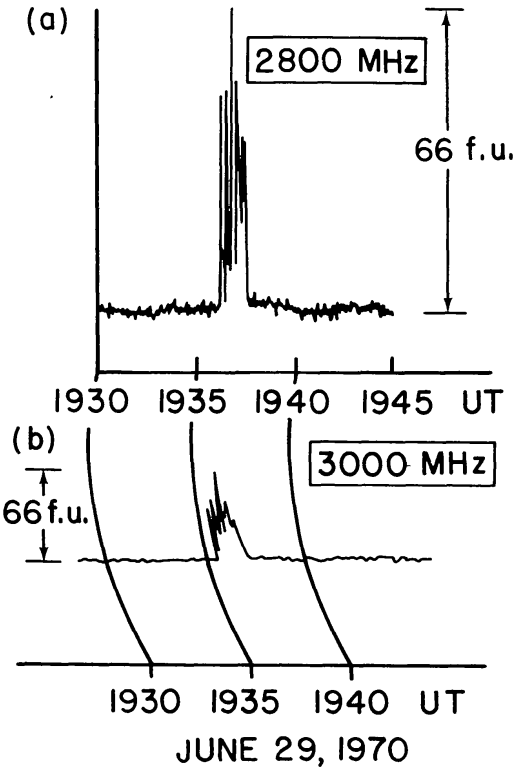

Fig. 8. Naval Electronics Laboratory record (a) of 29 June, 1970, confirming Aerospace's record (b) showing five peaks at 19 : 36.4, 19 : 36.6, 19 : 36.9, 19 : 37.3, and 19 : 37.6 UT, with pulse intervals of 17 s. Difference in pulse height is caused by difference in sensitivity of recorders. (*Note:* A 39-s timing correction in the 3000 MHz data has not been applied: the trace should be shifted to the right) (after Janssens *et al.*, 1973).

periodic or quasi-periodic pulsations in microwave bursts occurring at intervals of 10–20 s. These pulses are superposed on the impulsive phase of the burst (Figure 8), and often a series of small pulses occur on the top of a large rising or falling pulse. These ~ 10 s pulses appear to be more broadened than the ~ 10 ms pulses found by Slottje (see next section). These pulsations are not rare – they can occur during small, medium and large bursts. Sometimes, these microwave pulsations are coincident in time with strong meter-λ type III bursts. Such periodicities observed in hard X-rays, cm-λ and EUV must be directly related to acceleration mechanism itself or with wave modulation of particles that are accelerated by other means. This conclusion is partly supported by the findings of Gribbens and Matthews (1969) who showed that periodicities observed in radio bursts at 2800 MHz are related to the total energy of the burst.

The excellent correlation found by Parks and Winckler between 1.6 cm-λ and 60–112 keV X-rays in duration as well as in the burst structure (Figure 7) strongly implies that the source of these two types of radiation is common, that is, electrons of energies > 80 keV. On the other hand, the existence of more slowly varying X-ray and microwave components that are well-correlated indicates the presence of another energetic component.

(ii) *Time Structure with* 10–100 ms *Resolution*

Slottje (1978) observed a microwave outburst at 2650 MHz showing a strong and extremely fast fluctuating burst component. Many spikes appeared to have half-power durations smaller than the 20 ms resolution of the instrument used. These are about two orders of magnitude shorter-lived than events reported from previous microwave observations. They are only rivalled by fine structures seen in some decimeter type IV bursts observed between 0.4 and 1.0 GHz (Kundu and Spencer, 1963). The occurrence of microwave bursts with millisecond fine structure is not rare; Slottje observed several other examples, with similar fine structure. The associated Hα flares were important, ranging in importance from 2B to 4B. Slottje measured both left and right circularly polarized radiation (LCP and RCP), with an effective time resolution of 10 ms.

The first such microwave burst observed by Slottje consisted of a large number of successive spikes (see Figure 9a). Some of these showed millisecond structure. The

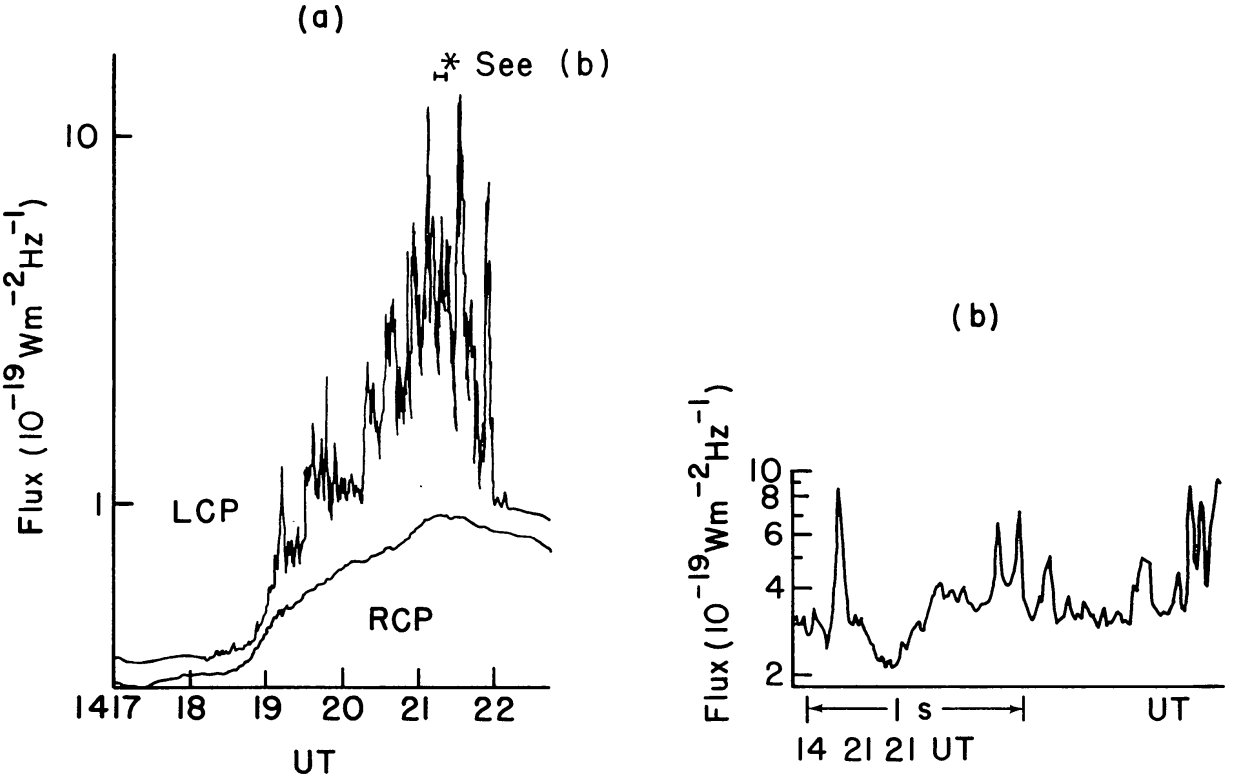

Fig. 9. (a) Flux density of both left (LCP) and right (RCP) circularly polarized components of the most variable part of the event. The fine structure is not resolved. (b) The indicated fragment (*) of about 2 s is expanded. Note that this is not one of the most intense peaks but rather a typical one (after Slottje, 1978).

general behavior at 2650 MHz (Dwingeloo) corresponds very well with that at 2800 MHz (Ottawa), but a sharp high frequency cutoff was observed during the whole event. The smooth component dropped by 3–5 dB, over only 150 MHz. The fluctuating component dropped by 5–7 dB over the same 150 MHz. The three major bursts (14 : 05, 14 : 20, and 14 : 40 UT in Figure 9b) at 2650 MHz showed a weakly L-polarized continuum, the first one without any spikes, the second one with a large number of 100% LCP spikes and the last one with sporadic or practically unpolarized spikes.

The spikes around 14 : 21 UT were 100% LCP. Flux densities of up to 6×10^{-19} Wm^{-2} Hz^{-1} were observed for nearly all durations. The occurrence of these spikes started along with the rise of the continuum, but ended rather abruptly (Figure 9a) long before the continuum ended. The half-power durations of the spikes were almost all (95%) below 40 ms, with the spikes of decreasing duration being more abundant. This implies that many spikes were not resolved.

An important consequence of the presence of millisecond structure in cm-λ bursts is that if the modulation in the emission is caused by a particle acceleration mechanism, it must be effective on time scales of milliseconds, which is 2 to 3 orders of magnitude shorter than envisaged in most models. The source dimensions were estimated by assuming a spatial growth rate between the Alfvén speed and the velocity of light. Assuming an Alfvén speed of ~ 3000 km s^{-1} (field strength ~ 300 G), a spike lasting 10 ms would have a source width between 30 and 3000 km. Such dimensions have been observed in microwave bursts although not all energy is contained in this compact core (Kundu *et al.*, 1974a, 1982a; Alissandrakis and Kundu, 1975).

The flux densities of the spikes, together with the source size estimates given above, lead to a lower limit of the brightness temperatures of $\sim 10^{15}$ K. Obviously a coherent radiation mechanism is necessary to account for such high brightness temperatures (see Section 4).

2.7. One-dimensional observations with arc sec resolution

Early high resolution observations of Kundu (1959) had shown that the centimeter burst source started with a size of slightly smaller than 1′, condensed into a smaller region ($< 1'$ arc) and then expanded to a size of $> 3'$ during the post-maximum decay phase. The burst was polarized mainly during the impulsive phase, the post-burst phase being essentially unpolarized. High resolution interferometric observations by Hobbs *et al.* (1974) and Kundu *et al.* (1974a) have provided valuable information on the existence of fine structure in the burst sources on scales of a few arc seconds. At 3.7 cm, the burst source often starts with a precursor of 4″ arc, condenses to a minimum size of 2″ arc at the peak of the burst, after which the source expands to a size of 5″ arc or larger. In a complex burst with several maxima, the burst sources are located at different positions (see Figure 10); this positional change is similar to the behavior of Hα flares which often have more than one maximum, each maximum corresponding to a small diameter 'kernel' (Alissandrakis and Kundu, 1975; Rust, 1976). One-dimensional fan-beam observations with a resolution of 6″ arc at 6 cm by Alissandrakis and Kundu (1978) have proved extremely valuable; they have confirmed the polarization and spatial characteristics of

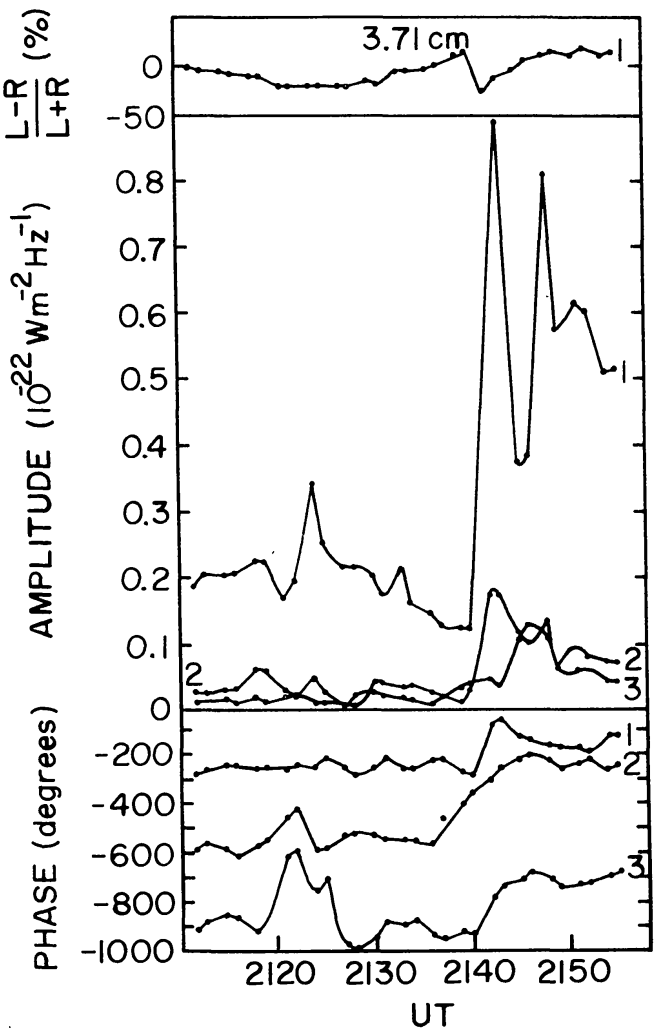

Fig. 10. Fringe amplitude, phase and circular polarization at 3.7 cm during a burst (after Alissandrakis and Kundu, 1975).

microwave bursts on a scale of several arc seconds and have revealed several other interesting features. Bursts of intensity 1 to 10 sfu (1 sfu = 10^{-22} Wm^{-2} Hz^{-1}) occur quite often near the neutral line of the magnetic field, as determined by the polarization maps of 6 cm active regions (Kundu *et al.*, 1977). At the time of maximum (impulsive phase), the source is most compact (size $\lesssim 10''$), it is strongly polarized and the brightness temperatures generaly exceed 10^8 K. After the maximum (post-burst phase), the burst core expands often with a velocity $\simeq 30$ km s^{-1} up to a size of $\geq 1'$ arc: it is unpolarized and the brightness temperature is generally $\sim 10^6$ K.

Marsh *et al.* (1979) used the partially completed VLA to observe several small flares at 6 cm. Their observations showed the presence of two distinct components: (1) A dominant broad component of size $\sim 10''$, $T_b \sim 1.5 \times 10^7$ K with gradual rise-and-fall behavior and 25–50% circular polarization, and (2) small impulsive components of size $\sim 2''$–$4''$, 53–98% circularly polarized. Using simultaneous observations with the Owens Valley interferometer at 2.8 cm they determined the location of the broad component in two dimensions. Comparison with Hα photographs and magnetograms

showed that this component was located in a magnetic arch at whose footpoints the Hα flare occurred. The electron temperature and emission measure estimated from simultaneous OSO-8 soft X-ray observations yielded a corresponding free-free microwave flux which, they believed, accounted for the observed emission at 2.8 cm. The microwave spectrum at longer wavelengths of 11 and 6 cm was shown by them to be consistent with thermal gyroradiation in a magnetic field of ~ 300 G; the burst source was believed to be a thermal cloud trapped in a magnetic arch. This is consistent with the first interferometric observations of microwave bursts by Kundu (1959) who interpreted the 'GRF''s at 3 cm-λ as due to thermal radiation. However, the temperature of the 'GRF''s were found to be only $\sim 10^6$ K, which could have been due to poorer resolution of 1′5 arc. Marsh *et al.* (1979) found that the flux and size of the impulsive bursts corresponded to brightness temperatures of $1–2 \times 10^7$ K, and spectral index of ~ 1.4 between 6 and 2.8 cm. Such a spectrum could be produced either by optically thin synchrotron emission from a power-law distribution of electrons ($N(E) \propto E^{-3.8}$) or by an optically thick thermal gyroresonance source whose effective area decreases with increasing frequency (Mätzler, 1978).

The strong circular polarization of the impulsive bursts is more difficult to interpret. Marsh *et al.* incorrectly interpreted it as due to the bursts occurring in a predominantly longitudinal magnetic field, which would result in a strong enhancement of the gyroresonance opacity in the extraordinary mode with respect to that of the ordinary mode. Such behavior is consistent with burst locations at the footpoints of the magnetic arch in which the main flare occurred rather than higher in the arch, as observed by Marsh *et al.* The sense of polarization at 6 cm was in all cases right circular, implying positive longitudinal field. The positional information derived from the VLA observations, together with the optical information, would then indicate that the impulsive bursts occurred at various places along the line defined by the positive-polarity footpoints of the magnetic corridor.

One important result found by Alissandrakis and Kundu (1978) was that only one sense of circular polarization was observed over the entire extent of the burst source. This implies that if the burst is associated with loop structures, the emission must be associated predominantly with one leg of the loop. The unipolar nature of the microwave source could be interpreted as evidence for the existence of asymmetrical bipolar magnetic fields in which the accelerated electrons are located (Kundu and Vlahos, 1979). The fact that no polarization is observed in the post-burst phase implies that the energetic electrons responsible for gyrosynchrotron radiation during the impulsive phase must be thermalized in the post-burst phase. The thermalization of the nonthermal electrons alone cannot explain the emission in the post-burst phase; there must exist at the same time an additional energization mechanism which will contribute to the post-burst phase emission.

2.8. Two-dimensional mapping of centimeter burst sources

Marsh *et al.* (1980), using the VLA at 6 cm with up to 1″ spatial resolution and 10 s time resolution produced a series of snapshot synthesis maps as a function of time. At the

times of peak emission, the burst sources appeared to be single, with sizes in the range 12″–18″. Comparison with H α photographs and magnetograms showed that the source was located between the H α kernels, close to the magnetic neutral line, in agreement with the results of Alissandrakis and Kundu (1978). Flux density spectra of these bursts in the range 1.4–35 GHz indicated that the spectral turnover at low frequencies could be caused by absorption by the ambient active region, either due to free-free absorption with $N_e \sim 10^{10}$ cm^{-3} or to gyroresonance absorption with $B \sim 400$–800 G. Synchrotron self-absorption has also been suggested to explain this spectral behavior.

Marsh and Hurford (1980) also used the VLA at 2 cm and 1.3 cm to produce two-dimensional images with resolution as high as 1″ × 0.75″. Comparison with optical data showed that in the impulsive phase, the microwave emission was dominated by a compact source (~ 2″) located between the H α kernels. In the post-impulsive phase, the microwave source became larger and elongated in a direction consistent with the orientation of the magnetic field lines joining the H α kernels. In one case, the microwave structure exhibited some correlation with the H α kernels, and formed a connecting bridge between them. Marsh and Hurford (1980) interpreted these results to imply that the initial energy release occurred near the top of the magnetic arch joining the H α kernels, and set an upper limit of 2″ for the size of the energy release region. A size of 2″ was obtained for a 3.7 cm burst observed by Kundu *et al.* (1974a) with corresponding brightness temperature of 8×10^9 K. However it was pointed out by Kundu (1981) that the burst source (of size 5″–10″) at 6 cm occupies a significant portion of both sides of the loop rather than being located at its top.

Using the VLA, Kundu and his collaborators (Kundu *et al.*, 1981a, 1982a, b) studied several impulsive 6 cm bursts and tried to relate their observations to those made in hard X-rays by HXRBS and HXIS experiments aboard the SMM and to interpret their results in terms of existing flare models.

(i) *Arcades of Loops as Sites of Primary Energy Release*

Kundu et al. (1982a) studied the impulsive phase of a flare observed on 25 June 1980 and showed how the VLA data could be used to provide information on the sites of energy release. This flare (H α/X-ray importance 1B/M2), showed a number of spatial components having several maxima superimposed on a rather broad impulsive background radiation. They synthesized 10 s 'snapshot' maps at 6-cm with a spatial resolution of 1″ × 2″ arc which clearly resolved the substructures of the burst source. They compared the locations and temporal variations of the radio burst components with simultaneous H α filtergrams and photospheric magnetograms.

As one can see from the samples of 10 s synthesized maps shown in Figure 11, the burst source is very complex; it consists of several component sources, the most intense of which is located near the center. The polarization (V) maps show that most of the burst components have bipolar structure. Several components, including the strong central source, have almost the same finite extent in total intensity and polarization (~ 5″ × 10″); the neutral line (6 cm) passes through the peak of total intensity and divides it into two regions of opposite polarity across the shorter extent of the region.

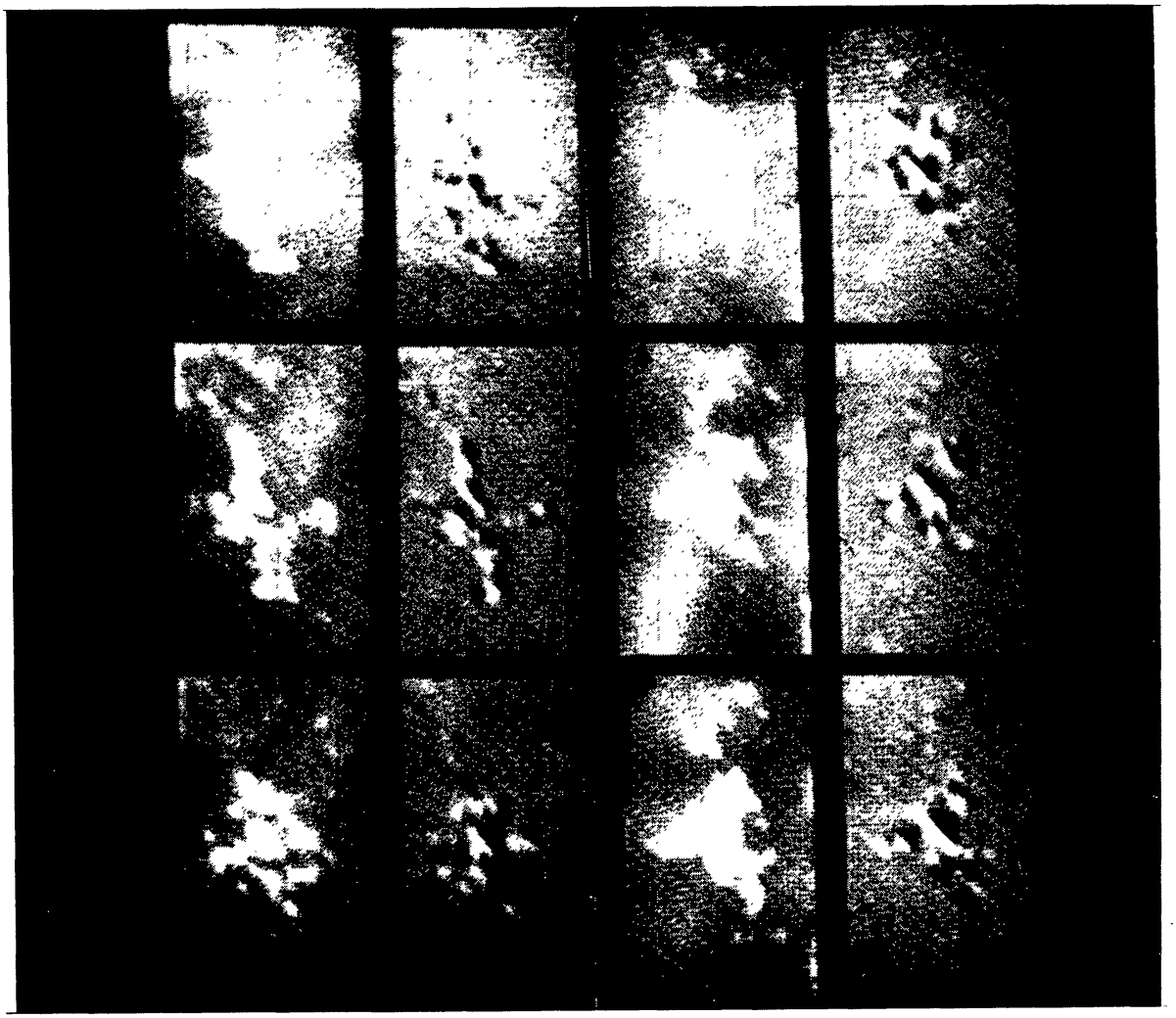

Fig. 11. Samples of 10^s snapshot maps of intensity (columns 1 and 3) and polarization (columns 2 and 4) during the burst of 25 June, 1980. Time runs down each column, starting at 15 : 52 : 45 in the upper left, ending at 15 : 53 : 35 in the lower right. Note the strong bipolar component in the midst of other bipolar components, indicating arcades of loops. At 15 : 53 : 25 the oppositely polarized footpoints are resolved into separate intensity peaks (after Kundu *et al.*, 1982b).

Kundu *et al.* (1982a) also compared the Hα flaring region at the time of each snapshot map and found that most of the optical emission occurs near the footpoints of the coronal loops seen in the burst radiation.

The emission from this complex (multiple-peak) microwave burst originates from a region consisting of several component sources, one of which is a strong dominant component located near the center of the complex. Most of these component sources appear in the form of arcades of loops, and the 6-cm emitting region occupies a substantial portion (5″–10″) on both sides of the flaring loop. There are, however, cases where the two opposite polarities correspond to two distinct, well resolved total intensity peaks, with minimal emission near the center. Several peaks of the June 25 burst components have similar polarization structure during their rise and fall. This indicates that, in this case, if the release of primary energy occurs by magnetic reconnection, it must occur on a local scale, within an individual loop. The energy must be deposited

throughout the loop in a time scale of $\lesssim 10$ s (the observational limit), since the peaks grow in this time scale.

(ii) *Current Sheet Between Closed Loops and Centimeter Wave Impulsive Bursts*

Kundu (1981) and Kundu *et al.* (1982b) discussed a set of VLA observations that pertains to changes in the coronal magnetic field configurations that took place in the various stages of the flare's evolution. The flare was observed on 14 May 1980, in association with an eruptive filament and the observations were made (Velusamy and Kundu, 1982) at 6 cm wavelength with a spatial resolution of $\sim 2''$ arc. The burst appears as a gradual component on which was superimposed a strong impulsive phase (duration < 2 min) in coincidence with a hard X-ray burst. Associated with the centimeter burst, there were a two-ribbon Hα flare of importance 2B and a soft X-ray burst (class M1).

The map of the pre-flare region (Figure 12a), showed intense emission with peak $T_b \sim 10^7$ K extended along a neutral line situated approximately in the east–west direction. A burst source of intense emission with $T_b \sim 40 \times 10^6$ K, appeared initially (Figure 12b), near the center at a location where a kink in the radio neutral line was observed earlier. The most remarkable feature of the burst source evolution was that an intense emission extending along the north–south neutral line (line of zero polarization) appeared (Figure 12d), just before the impulsive burst occurred. It may be significant that the impulsive burst occurred immediately following the development of this emission feature and that initially it was near this neutral line.

The sequence of 10-s snapshot maps of the impulsive phase (Figure 12e–h) shows the evolution of the magnetic structure that took place in this region before the peak of the impulsive phase. At the onset of the impulsive phase there was a relatively faint bipolar source which grew in intensity rather gradually; there was also a fainter elongated feature with $T_b \sim 100 \times 10^6$ K, apparently originating from an arcade of loops. Definite changes in the polarization structure occurred in this region before the peak of the impulsive phase. In the 20 s preceeding the impulsive peak this arcade of loops changed (see, Figure 12e–f) and ultimately developed into two strong bipolar regions or a quadrupole structure (at 19 : 19 : 55 UT, Figure 12g) whose orientations were such that near the loop tops the field lines were opposed to each other. It is important to note that this particular field configuration occurred just before the impulsive peak, and we believe that it was related to the impulsive energy release at its peak. This quadrupole field configuration is reminiscent of the flare models in which a current sheet develops in the interface between two closed loops. At the time of maximum (19 : 19 : 55 UT) the central compact source brightened to a high brightness temperature of $\sim 1100 \times 10^6$ K, with little change in its size. The impulsive energy release must have occurred near one of the centrally located neutral lines. The bright compact bipolar source is obviously related to the region of energy release by some kind of magnetic reconnection of the field lines originating from the two bipolar regions between which this compact region is located. Soon after the maximum, (Figure 12h) a loop-like structure with a lower brightness temperature ($< 300 \times 10^6$ K) developed around the compact source. The footpoints of the loop have predominantly opposite circular polarization. The two ribbon Hα flare occurred near the

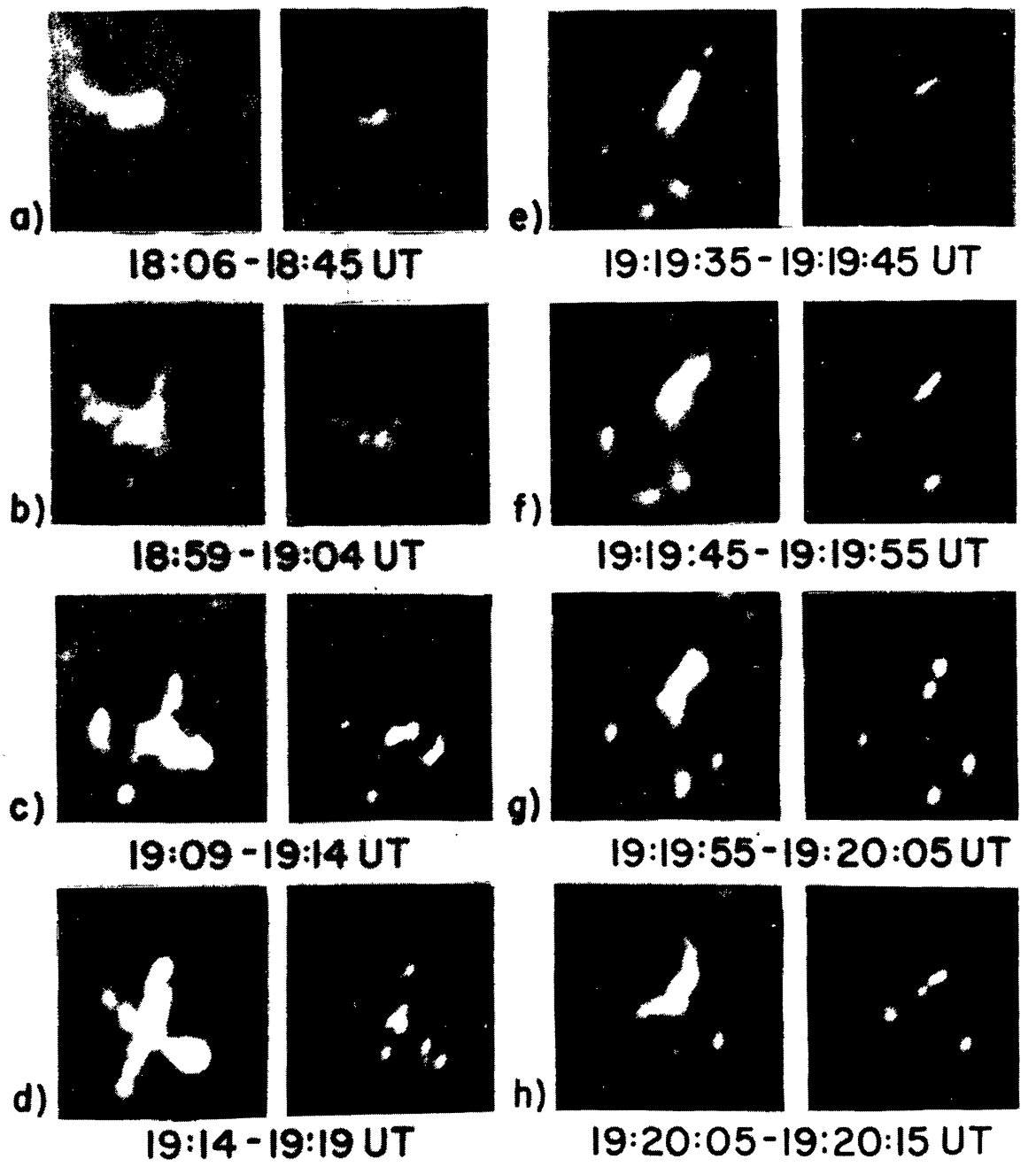

Fig. 12. Pre-flare active region and burst source maps for 14 May, 1980. Each map was synthesized from data taken during a time interval appropriate to the observed 6 cm flux. (a) Preflare 6 cm map 18 : 06–18 : 48 UT 14 May, 1980. Peak brightness temperature $T_b(\max) \sim 13 \times 10^6$ K. (b) Gradual phase of burst, 18 : 59–19 : 04. $T_b(\max) \sim 40 \times 10^6$ K. (c) Gradual phase of burst, 19 : 09–19 : 14. $T_b(\max) \sim 40 \times 10^6$ K. (d) Last 5^m map before impulsive phase, 19 : 14–19 : 19. (e) 19 : 19 : 35–: 45. Onset of the impulsive phase. $T_b(\max) \sim 100 \times 10^6$ K. (f) 19 : 19 : 45–: 55. Rise of the impulsive phase. (g) 19 : 19 : 55–20 : 05. Peak of the impulsive phase. Note the remarkable quadrupole structure. $T_b(\max) \sim 1100 \times 10^6$ K. (h) 19 : 20 : 05–20 : 15. Decline of the impulsive phase. $T_b(\max) \sim 300 \times 10^6$ K (after Kundu *et al.*, 1982b).

footpoints of the loop and the intense compact source was located near the top of this loop (Figure 13). The appearance of the north–south neutral line at the start of the impulsive phase must be indicative of the appearance of a new system of loops, possibly due to reconnections. The presence of two loop systems with opposite polarities must ultimately be responsible for the acceleration of electrons in the impulsive phase. The polarization map of Figure 12g, suggests such a possibility.

The source of burst radiation during the impulsive phase is very intriguing. A schematic diagram of the geometry of the burst source during the gradual and impulsive phases is

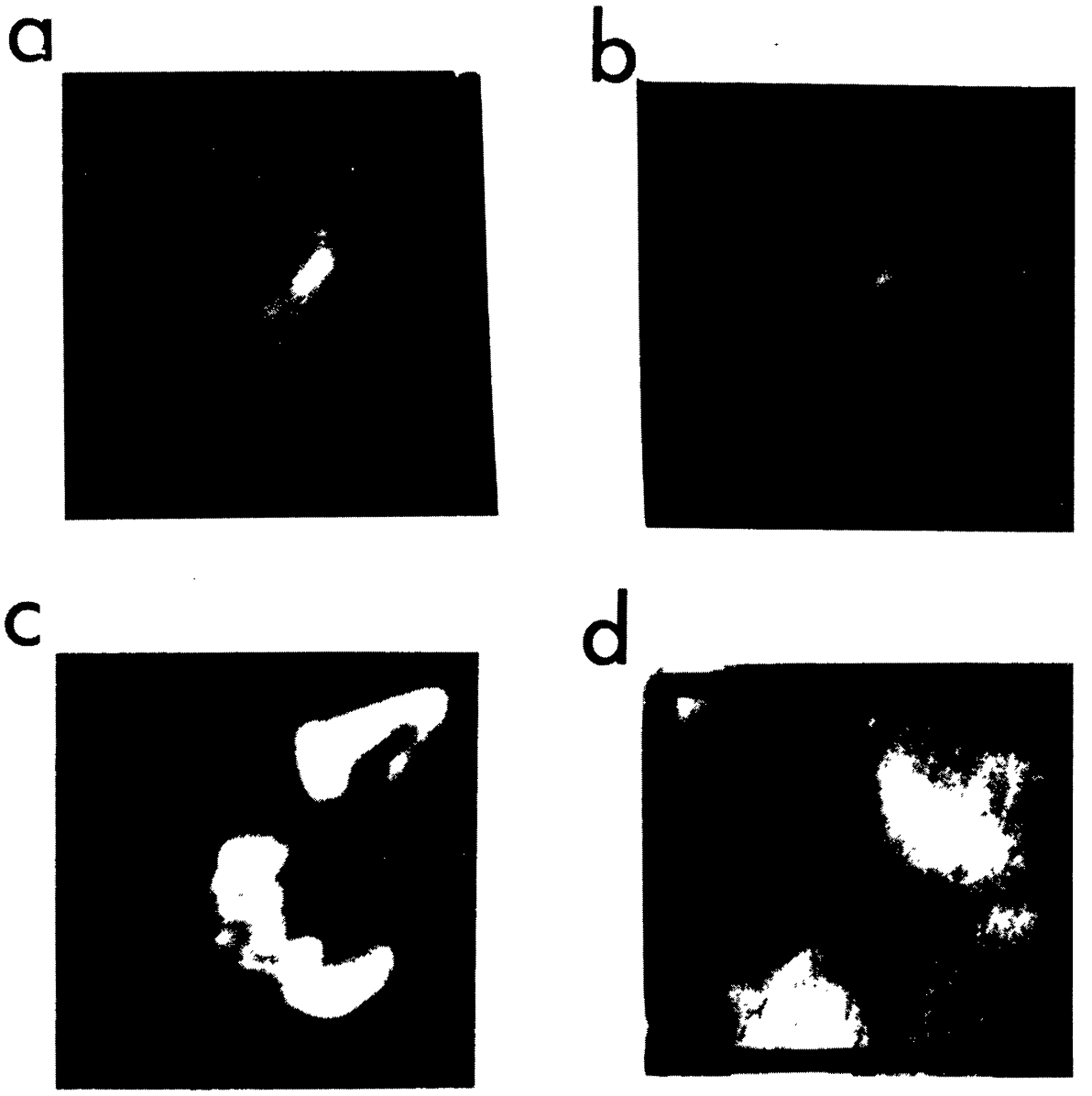

Fig. 13. The location of 6 cm radio burst with respect to Hα and magnetogram. (a) and (b) 6 cm map of total and polarized intensity at 19 : 20 : 15 UT; (c) Hα photograph at 19 : 20 : 13 UT (SOON data, courtesy, D. M. Rust); and (d) magnetogram at 18 : 44 UT (KPNO data, courtesy J. Harvey) (after Velusamy and Kundu, 1982).

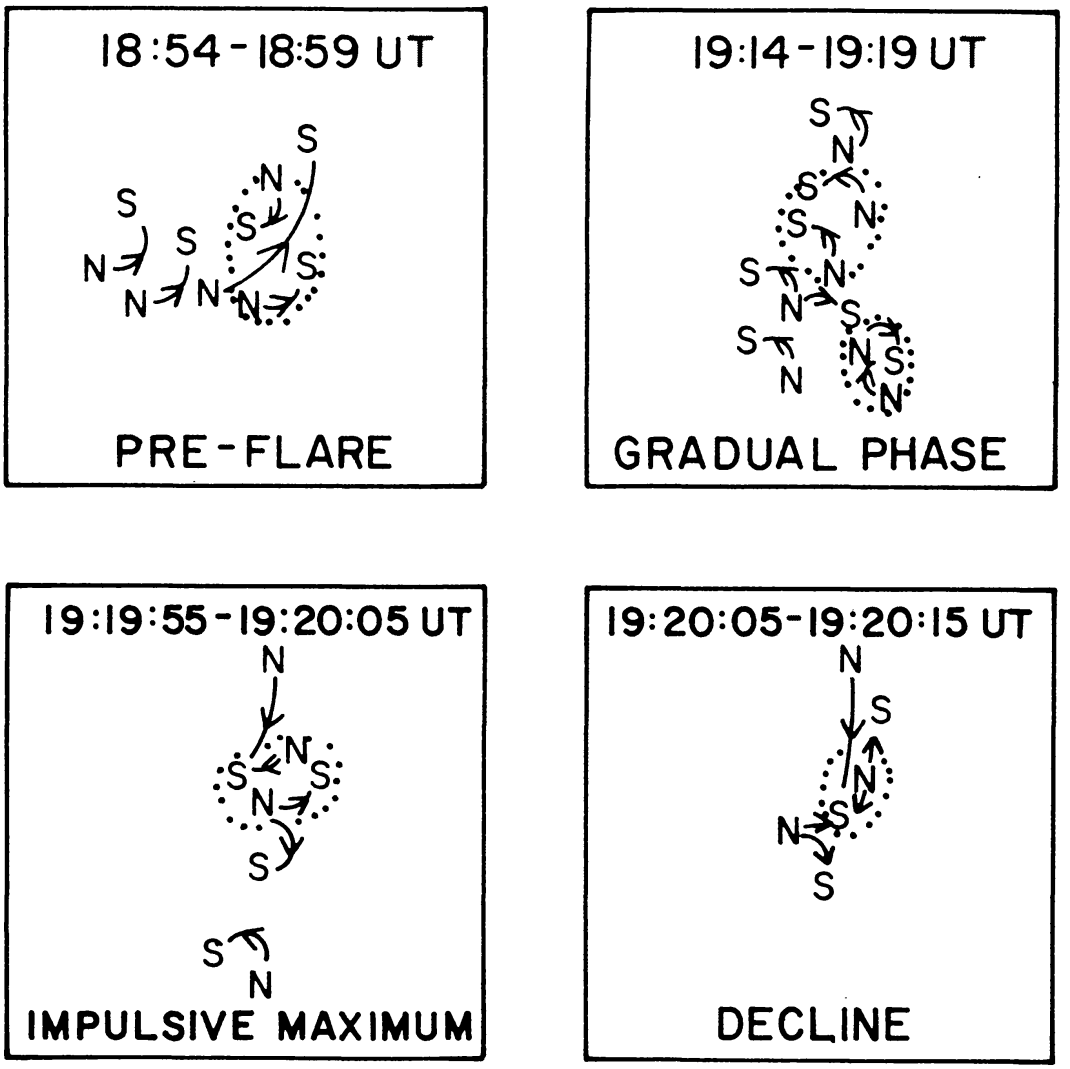

Fig. 14. Schematic diagram of the magnetic field structure in the burst source at selected times. The magnetic field configuration is inferred from the observed polarity of the 6 cm emission. The sketch at 19 : 19 : 55 shows one possible field configuration for the observed quadrupole. In each sketch the brightest components are shown encircled by a dotted curve (after Kundu *et al.*, 1982b).

presented in Figure 14. In this figure the magnetic field structures as inferred from the radio data at selected times, are shown.

Kundu *et al.*'s (1982b) study provided several examples of burst maps produced with the VLA, which appear to provide support for one or the other of the different classes of flare models. Few (if any) optical measurements are capable of distinguishing between flare models. (a) For a flare with multiple impulsive peaks emitted by independent, isolated bipolar magnetic structures, an isolated loop model is favored since the VLA polarization structure does not change during the rise and fall of the individual bipolar sub-sources. Frequently the emission from bipolar loops originates from a large part of the loop surrounding its top. There are also cases where the emission received from the footpoints is higher than that received from near the top. (b) For the onset of an impulsive burst (May 14, 1980) a quadrupole structure reminiscent of two bipolar loops in close proximity was observed for the first time; it was inferred that this configuration was

responsible for the triggering of the flare. It is possible that a neutral sheet developed in the interface between the two loops or that the interaction of two loops greatly influenced the current flow within the individual loops. The magnetic field topology of flaring regions, as inferred from VLA observations, appears to vary from one case to another. This diversity of field structures may imply the diversity of ways in which the magnetic fields can be dissipated in flares.

2.9. Correlation between cm-λ and X-ray bursts

(i) *Centimeter and Hard X-ray Bursts*

During solar flares, bursts of centimeter-wave radio emission are accompanied by bursts of X-radiation of both high (> 20 keV) and low energy (< 20 keV). The centimeter-wave bursts associated with high energy or hard X-rays are characterized by a sharp rise time and short impulsive phase. In one rare case observed on March 20, 1958, and associated with gamma ray (continuum) the cm burst was of very short duration ~ 20 s, and large angular size of $\sim 4'$ arc at 3 cm-λ (Kundu, 1959). Also, the spectra of centimeter-wavelength bursts associated with both hard and low energy or soft X-rays often show a rather sharp low frequency cutoff around 30 cm-λ, except when they are associated with bursts on meter waves. Type III bursts on meter wavelengths, which provide indications of the passage of electron streams through the corona, do not appear to be associated with high energy X-ray bursts in any significant manner (Kundu, 1961). On the other hand, there is a one to one correspondence between the occurrences of centimeter-wavelength and X-ray bursts (Kundu, 1961). The centimeter-wavelength maxima always coincide temporally almost precisely with the X-ray maxima, and sometimes there is agreement even in fine structure detail between the centimeter-wavelength and X-ray bursts, as discussed in an earlier section. The associated soft X-ray bursts are believed to be due to thermal bremsstrahlung. The occasional occurrence of meter-wave type III bursts at higher altitudes in the corona in association with hard X-ray bursts is probably due to the fact that some of the electrons produced during the flare escape in the upper corona, possibly as a consequence of an irregular flare structure (see Section 4). These electrons may excite type III bursts at higher levels in the corona, but they do not seem to play any significant role in the production of high energy X-rays (De Jager and Kundu, 1963). The accelerated electrons spend most of their time in regions where the field is largest and the pitch angle is the greatest. Thus, they tend to accumulate in the corona above the sunspots, and produce centimeter-wavelength bursts by gyrosynchrotron radiation. Electrons with small pitch angle not mirrored in the corona penetrate into the chromosphere and, produce X-radiation by collisional bremsstrahlung. The accelerated electrons lose their energy gradually by collisions and approach their thermal velocities, and so the X-ray spectrum undergoes a softening. This is quite consistent with the observed decrease of intensity and increase of angular size with consequent decrease of brightness temperature during the centimeter wavelength post-burst decay which is thermal in nature. For this reason, intensity variation of a centimeter-wavelength burst in its post-burst phase may not correspond closely to that of an X-ray burst, if we consider

only the high energy X-rays (say, > 20 keV). In this phase the intensity variation of a centimeter burst should correlate better to that of the associated X-ray burst in the lower energy (say, 1 to 10 Å) region.

It appears that a total of about 10^{34} fast electrons (energy > 20 keV) can account for the observed intensity of some X-ray bursts. If we consider that the X-ray burst has the same source size as the centimeter burst, that is, 0.1′ arc diameter or a volume of about 10^{26} cm^3, then there should be about 10^8 electrons per cm^3 of > 20 keV. This number is higher by about one or two orders of magnitude than the number of electrons of several hundred keV to produce the centimeter-wavelength burst by gyrosynchrotron radiation. This is not surprising since electrons with small pitch angles do not contribute to gyrosynchrotron radiation, but do produce bremsstrahlung bursts.

(ii) *Locations of Burst Peaks in a Multiple-peak Burst*

The hard X-ray burst intensity time profiles often show multiple peaks (spikes). Direct evidence on the question of origin of the multiple spikes in hard X-ray burst sources can only be obtained from hard X-ray images with spatial resolution as good as $\sim 1''$ arc. However, such resolution is presently not available with any space experiment, including the Solar Maximum Mission (SMM). Karpen (1980) made an extensive analysis of multiply-spiked hard X-ray bursts morphologically selected from OSO-5 data. Combining the parameters obtained from the hard X-ray emission (electron density, temperature and spectral index of electron distribution) along with the microwave spectra obtained at different peaks of a single burst, Karpen (1980) concluded that some multiply-impulsive bursts exhibited widely different magnetic field strengths at different times in their evolution, while in some burst sources the magnetic field strengths remained nearly the same. The magnetic field estimates were based upon the similarity or otherwise of the spectral shape, and the location in the frequency domain of the spectral peak (Figure 15a, b). These results imply that there are multiple-spike events whose component spikes appear to originate in one location, and there are events in which groups of spikes come from separate locations within the same active region, which flare sequentially. In order to investigate the locations of the multiple spike bursts, Kundu *et al.* (1981) adopted a different approach. Instead of finding the positions of the hard X-ray bursts, they determined the positions of 6 cm burst peaks corresponding to hard X-ray burst spikes with a resolution of 3″ arc using the VLA.

These bursts were all in the same region on the same day. Obviously their study involves determining the relative locations of the energetic electrons responsible for different peaks within a single 6 cm burst, although the associated hard X-ray emitting electrons may not be located at the same place. The direct observations using the VLA with a spatial resolution of 3″ of 6 cm bursts associated with four multiple-spike hard X-ray bursts (SMM-HXRBS data) confirm that at least in a set of 4 events analyzed by Kundu *et al.* (1981) the radio burst sources had the same location within $\pm 2''$ arc (Figure 16). The question then arises as to the origin of multiplicity of burst emission in a single source region. The simplest interpretation of different peaks in a single microwave burst is that each peak represents a new electron acceleration event. These

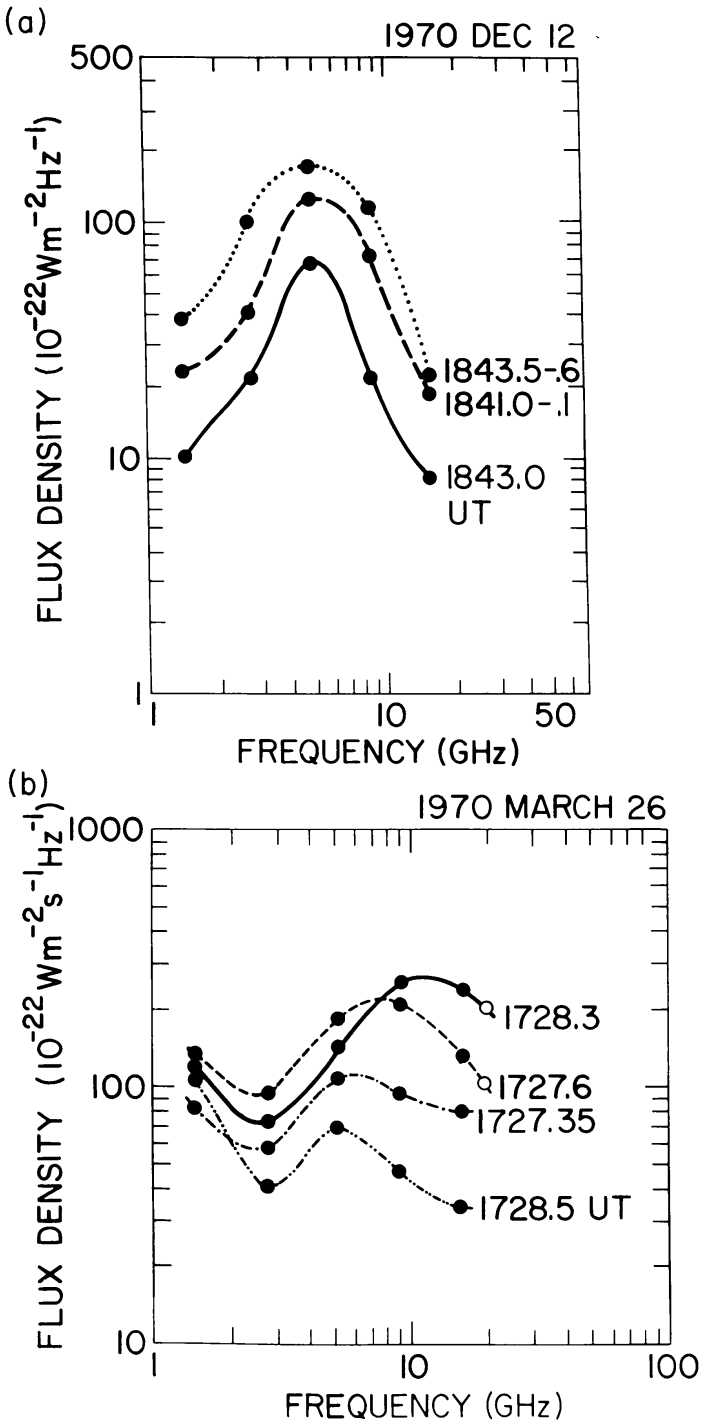

Fig. 15. (a) Microwave spectra at the times of peak intensity during the multiply-impulsive event of 1970, December 12. Note the consistency of spectral shape and turnover frequency. (b) Microwave spectra at the times of peak intensity during the multiply-impulsive event of 1970, March 26 (after Karpen, 1980).

accelerations could be due to the appearance of a separate population of electrons to produce the succeeding peaks or from repeated acceleration of one electron population. The case of reacceleration obviously necessitates a trap situation, in which the initial distribution of injected or released energetic electrons changes slowly enough for repeated accelerations to persist throughout the burst duration.

Kundu *et al.* (1981) pointed out that the sense of polarization is not always the same for different peaks within a single burst. A possible explanation for this phenomenon is

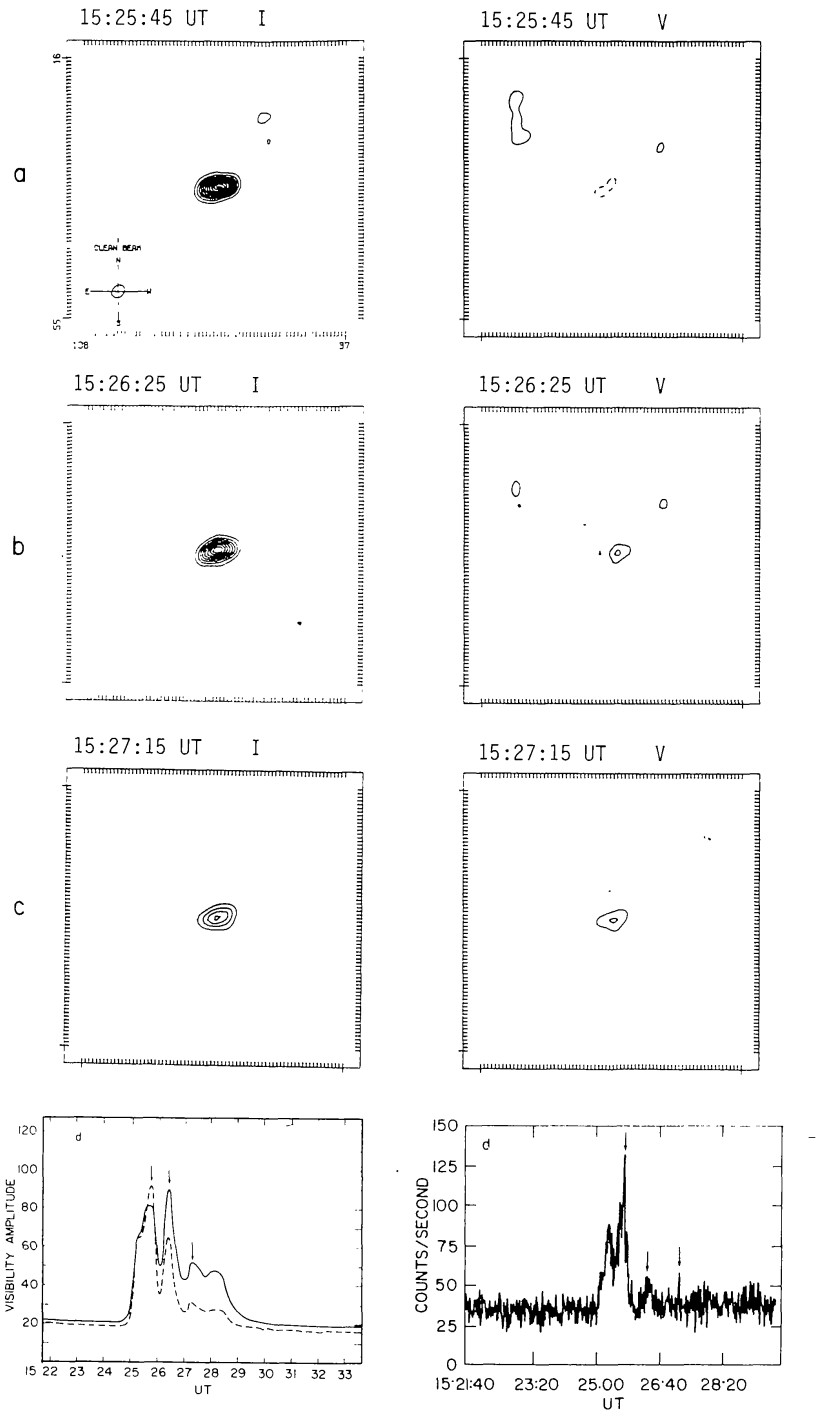

Fig. 16. 6 cm maps of the peaks of a multiple-spike burst shown in (d): (a) map of first peak, (b) map of second peak, (c) map of third peak. Right and left circular polarization are represented by solid and dashed contours. The field of view is 72″ × 72″. The lowest contours in the I and V maps are 2.6×10^7 K and 1.3×10^7 K in (a), (b), and (c). The contour intervals are the same as the lowest contours. (d) Time profile of the fringe amplitude (100 m baseline) for a 6 cm burst observed on March 30, 1980 starting at 15 : 24 UT (left); (right) corresponding hard X-ray (20–30 keV) time profiles (HXRBS data, courtesy of K. Frost). The solid line is for the right circularly polarized component and the dashed line is for the left circular polarized component. The arrows show the peak times at which microwave maps were made. These times correspond to the peaks or spikes indicated by arrows in the hard X-ray time profiles (after Kundu *et al.*, 1981).

that the magnetic field strength on two sides of a loop containing the radiating electrons undergoes variations in times of the order of a minute; this magnetic field variation will modulate the gyrosynchrotron radiation coming from the two sides of the loop corresponding to different polarities of the footpoints. Consequently we could observe one or the other mode of circular polarization at different peaks. The variation of field strength could be caused either by a travelling Alfvén wave from one footpoint to another or by differential spreading of the magnetic field at the two footpoints at the photospheric level. However, no detailed model has yet been suggested to account for these variations in the observed polarization structure.

(iii) *Impulsive* cm-λ *and Soft X-ray Bursts*

As mentioned earlier, soft X-ray bursts (e.g., in the band 2–12 Å) are often associated with cm-λ bursts. Spangler and Shawhan (1974) made a systematic study of the association of impulsive 2 cm-λ (15.4 GHz) bursts and soft X-ray bursts. They found that a large majority of impulsive microwave bursts (15.4 GHz) have accompanying 2–12 Å soft X-ray emission. Total duration and decay time for the X-ray bursts vary from a few minutes to several hours, while most of the cm bursts have a duration of only 2–3 min. A significant fraction of the X-ray events exhibit a flux enhancement prior to the main burst. This preburst enhacement usually lasts 5–10 min. The majority of the X-ray events begin simultaneously with or prior to the cm-λ burst, and the X-ray peak occurs simultaneously with or after the cm-λ burst. The average delay is about 2–3 min. The pre-burst X-ray flux increases are significantly correlated with the microwave flux increases, having a correlation coefficient of 0.43. In summary then, a soft X-ray burst starts with a precursor representing the heating of the region that flares up. This heating also shows up at short cm-wavelengths, as discussed earlier. The impulsive cm-λ and hard X-ray bursts start more or less simultaneously; the main soft X-ray burst may have an impulsive phase coincident with the cm-λ and hard X-ray bursts, but its rise time is slower. The soft X-ray burst goes through a second increase that lasts a much longer time (several minutes to tens of minutes), which depends upon the details of the acceleration mechanism and the parameters of the medium affecting the energy transfer from the energetic electrons to the surrounding plasma, e.g., collisional heating and 'evaporation' of the upper chromosphere (Somov, 1979). The soft X-ray burst then decays due to radiative cooling, conduction or expansion (see Section 4).

(iv) *Spatial Relationship of Microwave and Soft X-ray Burst Sources*

During the Skylab observing period, large sidereal interferometers were occasionally used for solar observations at cm wavelengths (e.g., the NRAO 3-element interferometer at 3.7 and 11.1 cm-λ, and the Stanford 5-element array at 2.8 cm-λ). With such instruments complete two-dimensional maps of cm-λ burst sources cannot be made. However, from the visibility and phase of the fringes observed during bursts at different baselines, valuable information could be obtained on the structure of the burst sources and the position of the flaring region relative to the core of the active region in which the burst occurs. If there are a large number of baselines one can in fact produce a one-dimensional

fan beam by combining the different interferometer outputs and get information on the structures and positions much more accurately (Kundu and Alissandrakis, 1975).

Since impulsive centimeter bursts are closely correlated with hard X-ray as well as soft X-ray bursts (Kundu, 1961; Kane, 1972), it is of interest to compare the spatial sizes and locations of the nonthermal flares with the thermal flares as observed in soft X-rays. Such a study was carried out by Kundu *et al.* (1976) for 3 bursts observed on August 9, 1973, using the NRAO interferometer with resolution of 3″ and 9″ at 3.7 and 11.1 cm and soft X-ray images obtained with the AS and E X-ray telescope aboard Skylab. A similar study was also carried out by Felli *et al.* (1975) and by Pallavicini and Vaiana (1976) using the Stanford array at 2.8 cm with a resolution of 16″ arc. Pallavicini and Vaiana studied the evolution of a single flare during the thermal decay phase, while Kundu *et al.* (1976) observed two flares (August 9, 1973) during the nonthermal impulsive phase, and also observed the decay phase of a third event.

Within the limit of uncertainties involved in the cm-λ and X-ray measurements, Kundu *et al.* found that the cm-λ burst source and the X-ray kernel were cospatial. The source sizes in the two spectral domains were also practically the same. It must be remembered, however, that only a fraction ($\sim 30\%$) of the total energy was emitted within the cm-λ structures of sizes of about 4–5″ arc (Alissandrakis and Kundu, 1975). This is because the NRAO interferometer could only measure sizes up to a maximum of $\sim 30''$ arc at 11.1 cm and $\sim 10''$ arc at 3.7 cm. The corresponding upper limit to the brightness temperatures of this extended component ranges from about 10^6 K to 3×10^6 K. One of the best studied ways of heating the flare plasma to X-ray temperatures is by collisional energy losses of 10–100 keV electrons in a thick target situation ((Hudson, 1973). The comparison of the spatial distribution of the nonthermal electrons as mapped by the cm-λ measurements with the soft X-ray distribution is particularly important since the soft X-ray kernels are possibly the same as the hard X-ray sources, since in a small flare the hard X-ray emission corresponds only to the impulsive phase of the associated soft X-ray burst. If the nonthermal electrons are confined to a loop and heat the soft X-ray emitting plasma by chromospheric evaporation at the loop footpoints, then we should expect the cm-λ region to be no larger than the X-ray emitting region. However, as reported by Alissandrakis and Kundu (1975) most of the 11.1 cm flux must come from sources of minimum size of $\sim 30''$ arc, well outside the structure of the X-ray kernel. This implies that a part of the impulsive cm-λ emission comes from a substantially larger area than either the X-ray kernel or Hα flare area. This is consistent with a central core which is well associated in size and position with the X-ray kernel and a diffuse extended halo. It should be pointed out that the August 9 events were rather unusual in that the soft X-ray kernels were the only structures observed during any of the three flares. Typically, kernels are accompanied and followed by larger diffuse structures (Kahler *et al.*, 1975). In the more typical case, the larger structure of the cm-λ bursts may have had a similar counterpart in the X-ray images.

As mentioned earlier, Felli *et al.* (1975) and Pallavacini and Vaiana compared the decay phase of a 2.8 cm burst with the soft X-ray burst. The 2.8 cm burst source was found to consist of two distinct components with angular size of $\sim 20''$–$30''$ but with

different evolution, one component decaying more rapidly than the other. The emission mechanism was thermal since the event showed a gradual decay evolution and had a low radio brightness temperature of $< 3 \times 10^6$ K compared to the electron temperature derived from the soft X-ray event ($\sim 10^7$ K). Only the component with rapid decay could be interpreted as associated with the X-ray event, as indicated by the coincidence of the observed radio flux decay and that derived from the expected free-free radio emission from the X-ray source. The more stable component which does not emit X-rays in the band 1–20 Å could be interpreted as a region of plasma with slightly higher electron density and lower electron temperature. The average values of the electron temperature and densities were found to be 8×10^6 K and 2.5×10^{10} cm^{-3}.

2.10. Summary

Concluding this section we summarize the status of the existing observational results as follows:

(a) The study of the flare precursor is an important contribution to the flare theory from microwave observations. It has provided evidence for the continuous build-up of magnetic energy in the lower corona prior to the flare. The two dimensional VLA maps in conjunction with detailed theoretical magnetic models for the preflare active region should prove to be extremely valuable for future research in this direction.

(b) There appears to be strong evidence in support of the theoretical arguments developed by Parker (1977) that the magnetic fields manipulated by the convection zone and the photospheric fluid motions are continually twisted, the twisted components rising up through the surface into the apex of each flux tube. The magnetic field lines try to reach equilibrium through reconnections, and in so doing heat the plasma and accelerate electrons. The interaction of this hot plasma or the energetic electrons with the magnetic field appears as microwave bursts (gradual or impulsive).

(c) The existing statistical spectra and polarization measurements support the view that the impulsive phase of the burst is most likely the signature of the gyrosynchrotron radiation emitted from the interaction of the energetic electrons with the preexisting magnetic field. In the post-burst phase, following the impulsive phase, the plasma is thermalized and the microwave emission does reflect this gradual change (e.g., the emission mechanism changes from gyrosynchrotron to collisional bremsstrahlung from thermal plasma).

(d) From the spectral characteristics of the microwave bursts one can get an approximate estimate of the magnetic field strength in the flaring region, ~ 300–400 G in the low corona.

(e) The time structure of the cm burst radiation reveals that the energy release process and the magnetic fields containing the energetic electrons vary in time; also the intense millisecond pulsations reveal the presence of micro-instabilities in the emitting region. We shall discuss these properties in more detail in the subsequent parts.

(f) The two dimensional mapping of cm burst sources using the VLA has provided new insight into the flare process: in complex burst sources having several maxima in the intensity time profiles, sometimes a number of distinct bipolar structures are

observed, on other occasions quadrupole structures have been observed. Thus we conclude (Kundu, 1981; Kundu *et al.*, 1982b) that we may have for the first time, evidence for two distinct processes for energy release in solar flares, e.g., isolated loops or colliding loops forming neutral sheets in their interaction region.

(g) We have reviewed the correlation of microwave bursts with bursts observed in other wavelengths domains, especially X-rays where the correlation is nearly 100%. Future theoretical flare models and theoretical work on the energy transport after the flare explosion will necessarily require detailed knowledge of this correlation.

3. Radiation Mechanisms for Microwave Bursts

3.1. General remarks

In the previous sections, we have described the principal characteristics of centimeter bursts, obtained from observations made over the past thirty years. Unlike the remarkable progress the observational techniques have made during this period, the progress in theoretical interpretations has been rather slow. This is a consequence of the fact that the magnetic structure and the velocity distribution of the radiating electrons in a flaring region are not well determined. In this section we shall discuss the basic properties of the radiation mechanisms believed to be responsible for the microwave burst emission. First, we shall summarize the emission and absorption properties of the plasma in the low corona in which the flare energy is released. We start with the well known radiative transfer equation in a magneto-active plasma.

In a nonuniform isotropic plasma, the radiation transfer equation is (Smerd, 1950)

$$\frac{\mathrm{d}}{\mathrm{d}\tau}\left[\frac{I_j(\omega)}{n_r^2(\omega)}\right] = \frac{I_j(\omega)}{n_r^2(\omega)} - \frac{J_j(\omega)}{a_j(\omega)}\frac{1}{n_r^2}, \tag{1}$$

where $I_j(\omega)$ is the intensity of the ordinary ($j = 1$) or extraordinary ($j = 2$) mode at frequency ω, $n_r(\omega)$ is the refractive index of the medium, $J_j(\omega)$ is the emission coefficient, $a_j(\omega)$ the absorption coefficient and τ_j is the optical depth defined by

$$\mathrm{d}\tau_j = -a_j(\omega)\,\mathrm{d}s\,, \tag{2}$$

where $\mathrm{d}s$ is a unit length along which the radiation is propagated. In stable plasmas

$$\frac{1}{n_r^2(\omega)}\left[\frac{J_j(\omega)}{a_j(\omega)}\right] = S_j^0\,, \tag{3}$$

where, according to Kirchoff's law, in the case of thermal emission the source function is given by:

$$S_j^0(\omega) = 10^{-40} f^2\,(\mathrm{Hz})\, T_e\,(\mathrm{K})\ \mathrm{Watts\ m^{-2}\ Hz^{-1}} \tag{4}$$

is the intensity of the jth component of equilibrium emission in vacuum. This means that

in stable plasmas only the emission coefficient $J_j(\omega)$ needs to be calculated and the absorption coefficient follows immediately from Equation (3). On the other hand, in unstable plasmas $a_j(\omega)$ and $J_j(\omega)$ are not related through Equation (3) and must be obtained independently.

By solving equation (1), we obtain the following expression for the power received from an emitting volume with characteristic length L_1

$$I_j(\omega) = S_j(\omega)\,[1 - e^{-aj(\omega)L_1}] + I_0 e^{-a^{\mathrm{th}}(\omega)L_2}\,, \tag{5}$$

where I_0 is the power emitted from the microwave source and propagating through the corona, $a^{\mathrm{th}}(\omega)$ is the absorption from the inner corona, L_2 is the length of the inner corona.

Another important term which is frequently used in the radio-astronomical literature is the so-called brightness temperature, defined as the equivalent temperature of a thermal source of size L that emits the power I observed at the Earth at frequency f and is given by the equation

$$I = \left(\frac{L}{R_0}\right)^2 \frac{1}{2\pi c^2}\, f^2\,(k_B T)\,,$$

where R_0 is the distance of the source from the Earth, or in commonly used units

$$T_b\,(\mathrm{K}) = 10^8\,[f\,(\mathrm{GHz})]^{-2}\, I\,(\mathrm{sfu})\,[L_9\,(\mathrm{cm})]^{-2}\,, \tag{6}$$

I is the power emitted from the source and L_9 is the size of the source in cm divided by 10^9. In the Sun if T_b is a few orders of magnitude above 10^6 K, we usually say that the radiation mechanism is 'nonthermal', since 'thermal' emission will produce brightness temperatures close to 10^6 K, i.e., the ambient coronal temperature.

We now give the expressions for the emission and absorption coefficients for the radiation mechanism that have been suggested to explain the different phases of a microwave burst.

3.2. Emission and Absorption Processes

Gyro-synchrotron emission is almost certainly the radiation mechanism for the broadband continuum spectrum in the *impulsive phase* of the burst. Electrons energized near the energy release region gyrate in the pre-existing magnetic field above the active regions, and radiate near the harmonics of the gyrofrequency $\Omega_e = |eB/mc|$, where B is the magnetic field strength in the emitting source and m, e are the mass and charge of the electron. The emission coefficient $J_j(\omega)$ is given by the expression (Trubnikov, 1958)

$$J_j(\omega) = \int \mathrm{d}^3\bar{p} f(\bar{p}) \eta_j(\bar{p}, \omega)\,, \tag{7}$$

where $\eta_j(\bar{p}, \omega)$ is the emissivity of each electron given by

$$\eta_j(\bar{p}, \omega) = \frac{e^2\omega^2 n_r}{2\pi c} \sum \left\{ \left(\frac{\omega \cos\theta - n_r \beta_\parallel}{n_r \sin\theta} \right)^2 J_s^2(a) + \beta_\perp^2 J_s'^2(a) \right\} \delta(b) \tag{8}$$

$a = (\omega/\Omega_e)\beta \sin\theta$, $b = s\Omega_e - \omega(1 - \beta_\parallel \cos\theta)$, $\beta = v/c$, $\beta_\perp = v \sin\phi/c$, $\beta_\parallel = v \cos\phi/c$, J_s is the Bessel function, θ is the angle between the wave vector and the direction of the magnetic field, and ϕ is the pitch angle.

It is obvious from Equations (7) and (8) that two factors play important roles in the emission: (1) the velocity distribution of the radiating electrons and (2) the strength of the ambient magnetic field with which the electrons interact.

The absorption coefficient is given by the equation

$$a_j(\omega) = -\frac{8\pi^3 c^2}{\omega^2 n_r^2} \int \eta_j(\bar{p}, \omega) \frac{\partial f}{\partial \varepsilon} \, \mathrm{d}^3\bar{p} \,, \tag{9}$$

where $\varepsilon = p^2/2m$.

The absorption coefficient depends strongly on the details of the velocity distribution and its evolution in time. Two basic types of velocity distributions are usually postulated in the models that are used to explain the microwave burst radiation (see next section): (a) a Maxwellian $f_m(T_e)$ and (b) a Maxwellian for the ambient plasma and a streaming velocity distribution f_s for the electrons injected in the emitting volume from the energy release region i.e., $f = f_m + f_s$. In the latter case the streaming distribution f_s (which for the moment is assumed to be stable against plasma instabilities) dominates in the emission of the microwave burst. But many different sources can contribute to the absorption coefficient, namely, gyroresonance absorption (a_{th}) by the magnetized ambient plasma, self-absorption a_{sa} by the streaming electrons themselves, free-free absorption (a_{ff}) by collisional damping of the emitted radiation which is the opposite of the bremsstrahlung emission and finally the Razin effect arising from the change in the dielectric properties of the cold plasma inside the emitting region. In this section we shall assume a constant magnetic field to describe the characteristics of the radiation spectrum, using the above velocity distributions. This assumption is supported by the fact that recent high resolution observations, discussed in the previous sections, indicate that at the *impulsive phase* the microwave source is compact with characteristic size 2″–4″ (i.e., $< 10^9$ cm). We assume that the magnetic field does not change significantly over these lengths. We also discuss qualitatively the possible effect of steep magnetic field gradients on the radiation spectrum.

(i) *Gyro-Synchrotron Radiation from an Ensemble of Electrons with Maxwellian Velocity Distribution*

The gyro-synchrotron radiation from a thermal plasma has been discussed extensively in the literature (see for example, Zheleznyakov, 1970, with particular reference to plasma with coronal temperatures; Drummond and Rosenbluth, 1963, for much higher temperatures e.g., $T \simeq 10^8$–10^9 K in connection with fusion reactors; Matzler, 1978; and Dulk

et al., 1979, for microwave bursts). The basic characteristics of the spectrum of a thermal plasma are summarized below.

Using Equations (7), (8), and (9) for a Maxwellian velocity distribution we find (Bekefi, 1966)

$$J^j_\omega\left(\frac{\pi}{2}\right) = \left(\frac{\omega_e^2}{\Omega_e c}\right)\left(\frac{\omega^2 kT_e}{8\pi^3 c^2}\right)\sum_m \phi(m; x; \mu)\,, \tag{10}$$

$$\alpha^j_\omega\left(\frac{\pi}{2}\right) = \left(\frac{\omega_e^2}{\Omega_e c}\right)\sum_m \phi(m; x; \mu)\,, \tag{11}$$

$$\phi(m; x; \mu) = (2\pi)^{1/2}\,\frac{\mu^{5/2}}{x^4}\,m^2(m^2 - x^2)^{1/2}\,e^{-\mu}\left(\frac{m}{x} - 1\right)A^j_m\left(\frac{m}{x}\right), \tag{12}$$

where $x = \omega/\Omega_e$, $\mu = (m_0c^2/kT_e)$, $m = 1, 2, \ldots$ are the contributions for different harmonics, $j = 1, 2$ for the ordinary and extraordinary modes and A^j_m for midly relativistic electron ($m\beta < 1$)

$$A^j_m = \frac{(m\beta)^{2m}}{(2m+1)!}\left(\frac{\beta^2}{2m+3};\ 1\right). \tag{13}$$

The first term in the parenthesis refers to $j = 1$ and the second term to $j = 2$. For a slab of length L of a few thousand kilometers, density $N_e \simeq 10^{10}\,\mathrm{cm}^{-3}$, magnetic field $B = 100$ G and electron temperature $T_e \sim 10^8$ K we plot the optical depth $\tau_2(\omega/\Omega_e)$ for different angles θ (Figure 17a) and the harmonic number m^* for which $\tau_2 = 1$ (Figure 17b). For temperature $T \simeq 10^8$–10^9 K the results of Figure 17b can be approximated by the simple relation for $\theta \simeq \pi/2$ (Dulk *et al.*, 1979),

$$\tau_2 = 5 \times 10^3\,T_8^7 \sin^6\theta (N_{10}L_8/B_2)B_2^{10} f_9^{-10} \tag{14}$$

$$\tau_1 \simeq \beta^2\tau_2 \tag{15}$$

$$m^* = 9T_8^{0.7}\,. \tag{16}$$

Changing from m^* to $f_{\max}$ which occurs at $\tau \simeq 2.5$ and $\omega/\Omega_e \simeq 0.9m^*$ we have

$$f_{\max} \simeq 2.4(N_{10}L_8/B_2)^{0.1} \sin^{0.6}\theta T_8^{0.7}B_2 \tag{17}$$

in GHz. From Equation (15) we see that the gyro-synchrotron absorption coefficient for the *o*-mode is smaller than the *x*-mode by a factor of 0.3 for $\theta = 75°$. Thus at low frequencies, where the source is optically thick for both modes, the net polarization is calculated to be zero. At higher frequencies $\tau < 1$ the degree of polarization is calculated to be as high as 90% for $\theta = 45°$. For $f > f_{\max}$ the spectrum falls rapidly as f^{-a} where $a = 10$–12 (see Figure 18). The spectrum for $f < f_{\max}$ will be modified if magnetic field or temperature gradients exist e.g., if the microwave source is cospatial with a reconnect-

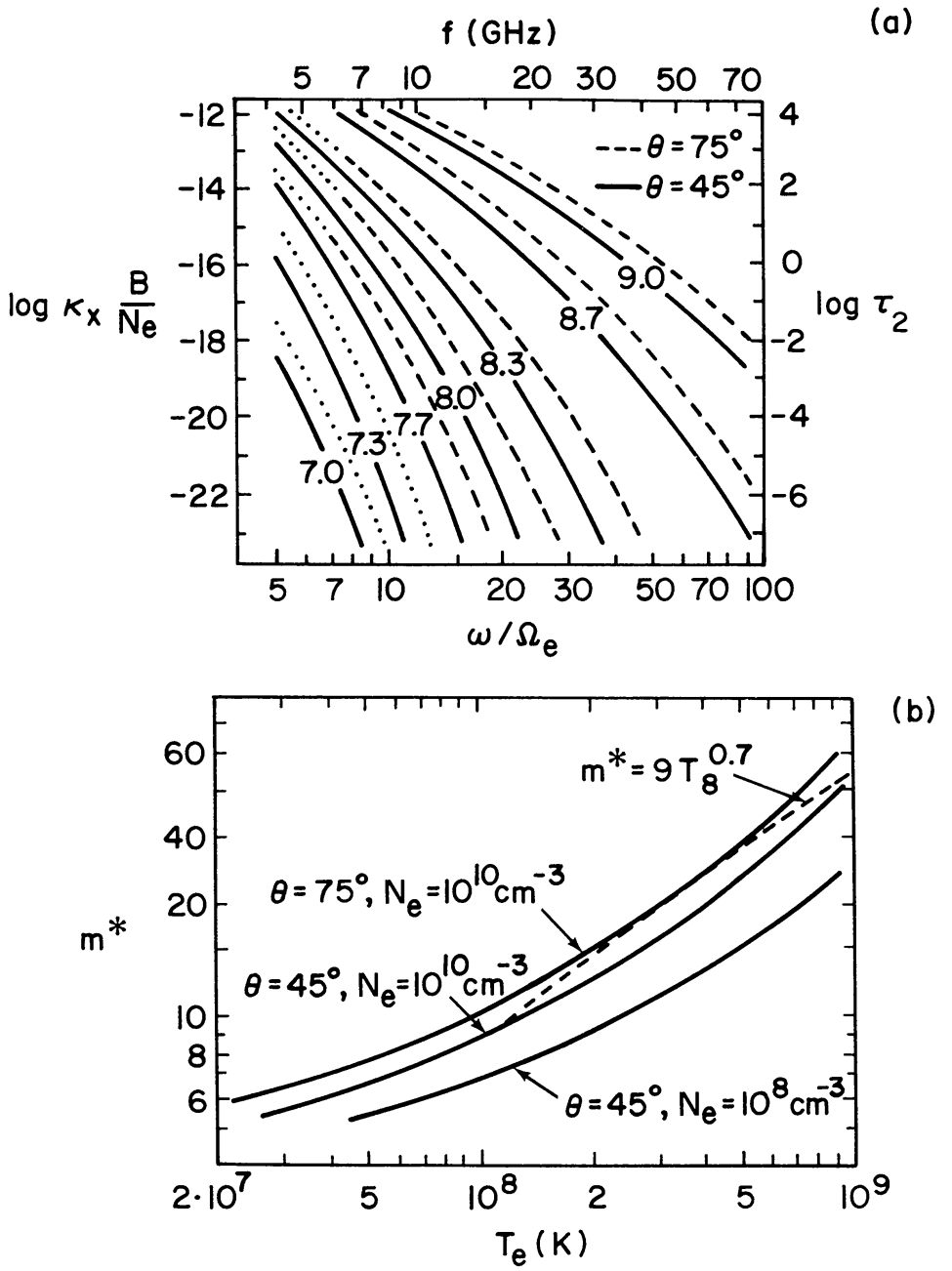

Fig. 17. (a) The gyromagnetic absorption coefficient for the extraordinary mode from numerical computations for two values of θ and seven values of T_e. The shortened dashes indicate the general trend in regions where there is fine structure because the influence of individual harmonics is not entirely wiped out by Doppler shifts. When calculating the refractive index f_e = 900 MHz ($N_e = 10^{10}$ cm^{-3}) and f_B = 840 MHz (B = 300 G) were assumed. The right and top scales show the optical depth τ_2 and microwave frequency, respectively, for such a source with scale length L = 2000 km. (b) The harmonic number m^* for which $\tau_2 = 1$, for the indicated values of θ and n_e; a scale length L = 2000 km was assumed. The dashed line between $10^8 \leq T_e \leq 10^9$ K shows the approximation used in the text (after Dulk *et al.*, 1979).

ing x-neutral point. In Figure 18 we show the effect of steep magnetic field gradients in the spectrum (Matzler, 1978).

On the basis of the theoretical considerations presented here we conclude that the statistical spectra of the majority of microwave bursts in the impulsive phase are not consistent with the simple form of the thermal interpretation since the majority of the

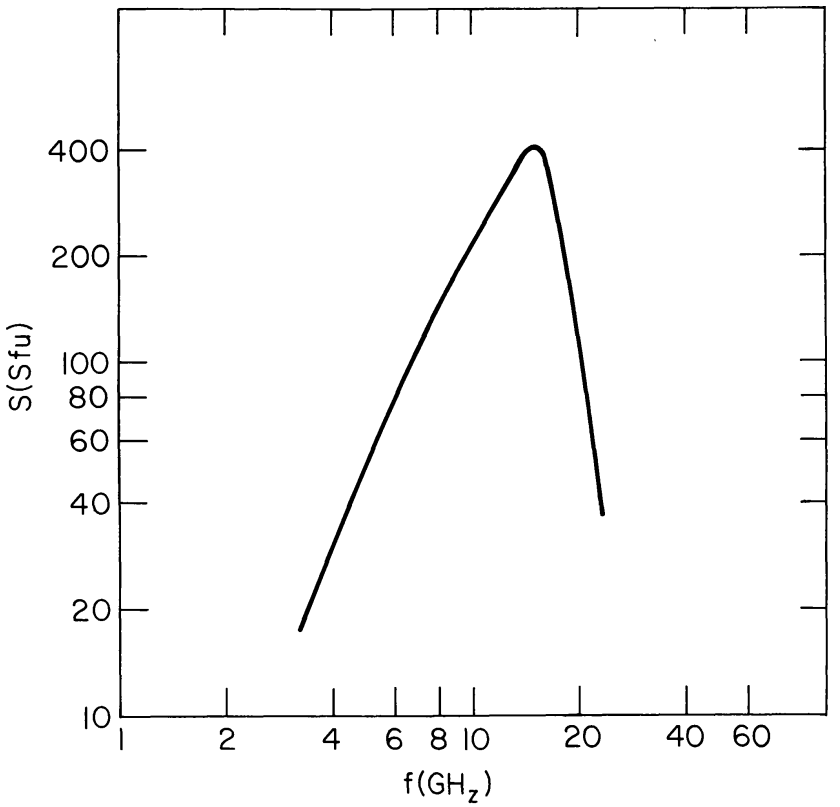

Fig. 18. Spectrum for a thermal source with $T_e = 2 \times 10^8$ K, $N = 8 \times 10^8$ and $B = 370$ G (after Dulk *et al.*, 1979).

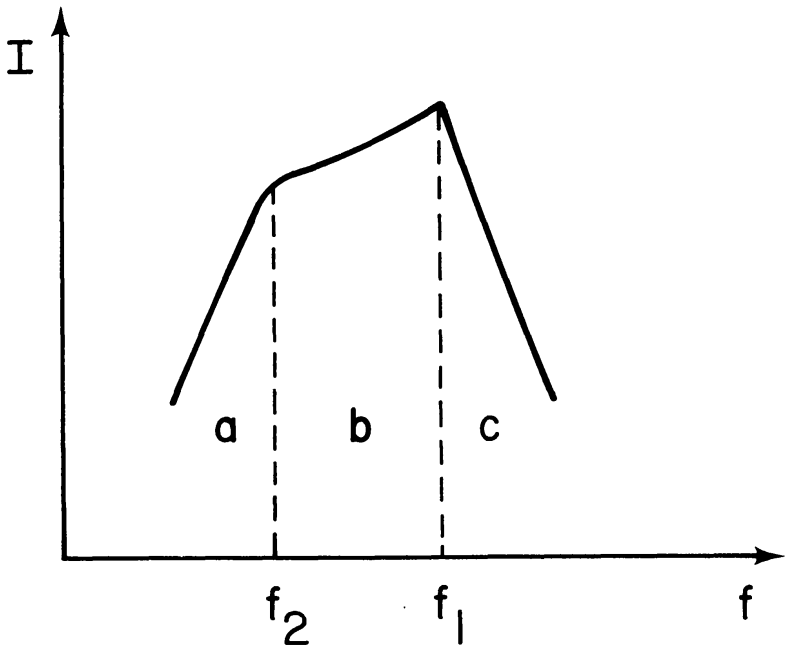

Fig. 19. Schematic microwave spectrum from a thermal plasma in a varying magnetic field. (a) Shows the black body part of the spectrum with polarization near zero. (b) The radiation comes from optically thick and thin region and the polarization is around 10–20% and (c) the optically thin part of the spectrum with polarization around 100%. Arbitrary units are used.

known spectra given by Guidice and Castelli (1973) have slopes $a = 3$–4 at high frequencies $f > f_{max}$ and the polarization is 10–40%, much less than what is predicted from a thermal distribution.

There are also several other difficulties in confining a thermal source with $T_e \sim 10^8$–10^9 in a magnetic loop; we shall come back to this problem in Section 4. It is important at this point to note that in the post-burst phase (a few minutes after the peak in intensity) or for gradual rise and fall burst the thermal interpretation is usually in accordance with the observations (Kundu and Vlahos, 1979).

(ii) *Gyro-Synchrotron Radiation from an Ensemble of Mildly Relativistic Electrons with Power Law Velocity Distribution*

The velocity distribution in a radiating region in this case is given by

$$f = f_m + f_s\,, \tag{18}$$

where $f_s \sim v^{-2\gamma}\phi(q)\theta(v_c - v)$, $\phi(q)$ is the pitch angle distribution of the energetic electrons, and θ is the step function. The streaming electrons are injected into the low corona from the energy release region and f_m is the local Maxwellian. The gyro-synchrotron

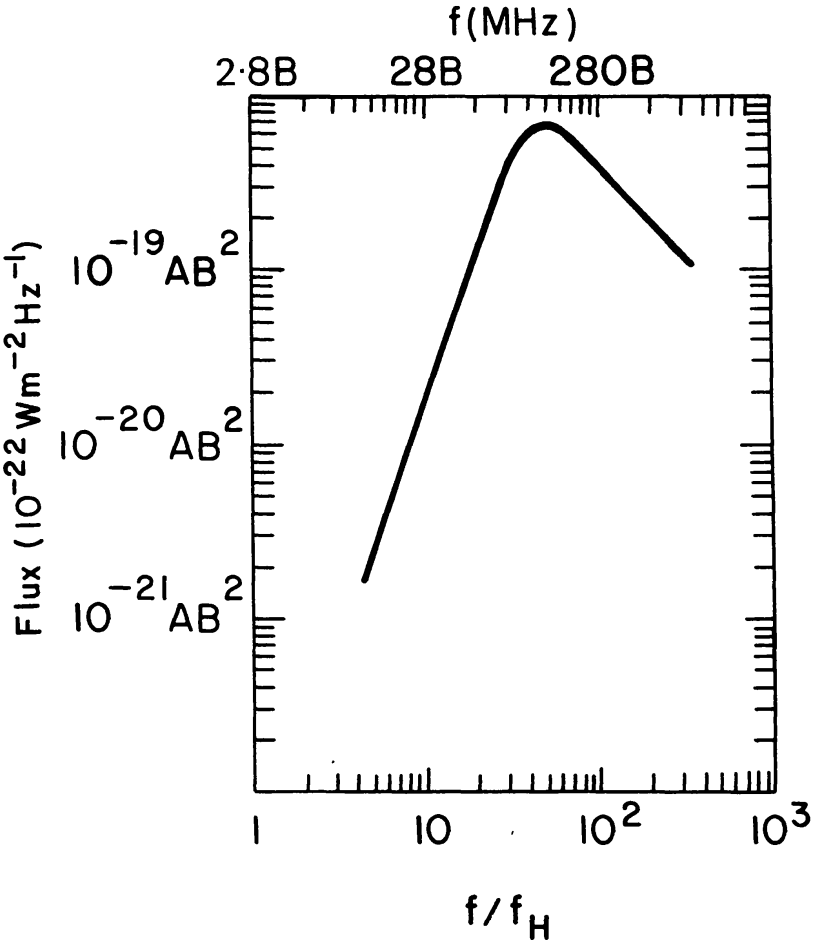

Fig. 20. Theoretical radio spectra for a uniform magnetic field and a power law velocity distribution with $\gamma = 3$, and $\theta = 45°$ (after Ramaty, 1969).

radiation for this velocity distribution has been extensively discussed in the literature (see Ramaty, 1973, and references herein). We summarize the basic conclusions here.

The spectrum, as shown in Figure 20 rises up to a maximum intensity at frequency f_{max} and gradually falls off as f^{-a} for $f > f_{max}$. The exponent a is related to γ with a simple relation, $a = (\gamma - 1)/2$ and the polarization for $f > f_{max}$ is given by the expression (Ginzburg and Syrovatskii, 1965)

$$P(\%) = \frac{\gamma + 1}{\gamma + 7/3} . \tag{19}$$

It can reach as high as 75% in the extraordinary mode for $\gamma \simeq 3$. Unlike the thermal velocity distribution the expressions for the emission and absorption coefficients for a power law velocity distribution cannot be given analytically in closed form.

(a) *Gyro-resonance absorption.* The magnetized thermal plasma inside and outside the radiating region will reabsorb the emission at the first two harmonics of the gyro-frequency Ω_e. The optical thickness estimated by the Equations (2) and (9) and a Maxwellian velocity distribution is given by the simplified relation (Zheleznyakov, 1970)

$$\tau_{j,\,s=1} = \tau_{j,\,s=2}$$

$$\tau_{j,\,s\geq 2} = \frac{s^{2s}}{2^{s-1}s!}\left(\frac{\omega}{c}\right)\left(\frac{\omega_e}{\omega}\right)^2\left(\frac{v_e}{c}\right)^{2s-2} L_H , \tag{20}$$

where we assumed that $n_r \simeq 1$ and $\cos\theta = 1$, v_e is the thermal velocity and $L_H \simeq \Omega_e \left| dl/d\Omega_e \right|$ is the scale length over which the magnetic field changes outside the radiating region ($L_H > 10^9$ cm). The main conclusion is that the gyro-resonance absorption will cause very sharp attenuation of electromagnetic waves of frequency Ω_e, $2\Omega_e$ and possibly $3\Omega_e$ in a direction where $\cos\theta \simeq 1$. Thus if gyro-resonance is the dominant absorption mechanism for the microwave source, the maximum frequency f_{max} is given by

$$f_{max}^{th} \sim 4 f_H \tag{21}$$

if one assumes that $N \leq 10^{10}$ cm^{-3} and $T_e \sim 10^7$ K in the thermal plasma in the vicinity of the emitting source. As we emphasized in Section 2, this relation permits us a quick estimate of the average magnetic field in the emitting source.

(b) *Razin effect.* Until now we have assumed that the index of refraction $n_r = 1$. For a cold plasma

$$n_r^2 = 1 - \left(\frac{\omega_e}{\omega}\right)^2 . \tag{22}$$

As we can see from Equation (8) the index of refraction can influence both the propagation as well as the emission of gyro-synchrotron radiation. The standard method usually employed to calculate the emitted power from an ensemble of electrons, namely to sum up the radiation of each individual electron as if it was in vacuum is incorrect (especially for frequencies $f < f^R$, where f^R is given below) since the radiation of the same electrons in the presence of plasma will be different. Takakura (1972) gave an approximate formula for frequencies above which the suppression of the radiation due to Razin effect is unimportant, namely

$$f > f^R_{\max} \left[\gamma \frac{\omega_e^3}{\Omega_e} \right]^{1/2} \tag{23}$$

for midly relativistic electrons.

(c) *Free-free absorption.* The emitted electromagnetic radiation can be absorbed collisionally by the surrounding plasma if it is dense ($N > 10^{11}$ cm^{-3}) or clumps i.e. $x = \langle N^2 \rangle^{1/2} / \langle N \rangle$ is locally a large number. The maximum frequency $f_{\max}$ in the case where free-free absorption is the dominant absorption mechanism is given by (Ramaty and Petrosian, 1972)

$$f^{ff}_{\max} = 0.4 \langle N \rangle L^{1/2} T_e^{-3/4} x \,, \tag{24}$$

where $\langle N \rangle$ is the average density and L the characteristic length of the dense layer and T_e its temperature.

(d) *Self-absorption.* Finally in cases where the number of streaming electrons, $N_s = \int f_s \, dv$, becomes very large they can emit and absorb the electromagnetic radiation from another part of the source. The self-absorption depends strongly on the number of the energetic electrons N_s, the length of the emitting source and the magnetic field. Ramaty and Petrosian (1972) gave a simple relation for the maximum frequency

$$f^{sa}_{\max} = 10^{12.5} I_m^{2/5} B_\perp^{1/5} \,, \tag{25}$$

where I_m is in erg cm^{-2} s^{-1} Hz^{-1} sr^{-1}. One important factor overlooked by Ramaty and Petrosian (1972) and by Takakura (1972) is that the number of streaming electrons will be restricted by plasma instabilities which will be excited if N_s is large. Vlahos and Papadopoulos (1979) have studied the beam plasma instability in the low corona and concluded that beams are stable only if $N_s < 10^{-2} N$. This restriction coupled with new estimates of the length of the radiating region $L \sim 10^8$–10^9 cm undermine considerably the importance of self-absorption at high frequencies ($f > 5$ GHz).

In summary we conclude that the emission from a Maxwellian plus a power law tail is dominated by the tail; however, the bulk of the distribution can play a very important role in absorption or emission since all three basic absorption processes e.g., gyro-resonance absorption, Razin supression and free-free absorption, depend strongly on the parameters of the bulk of the plasma. In Figure 21 we demonstrate how self-absorption

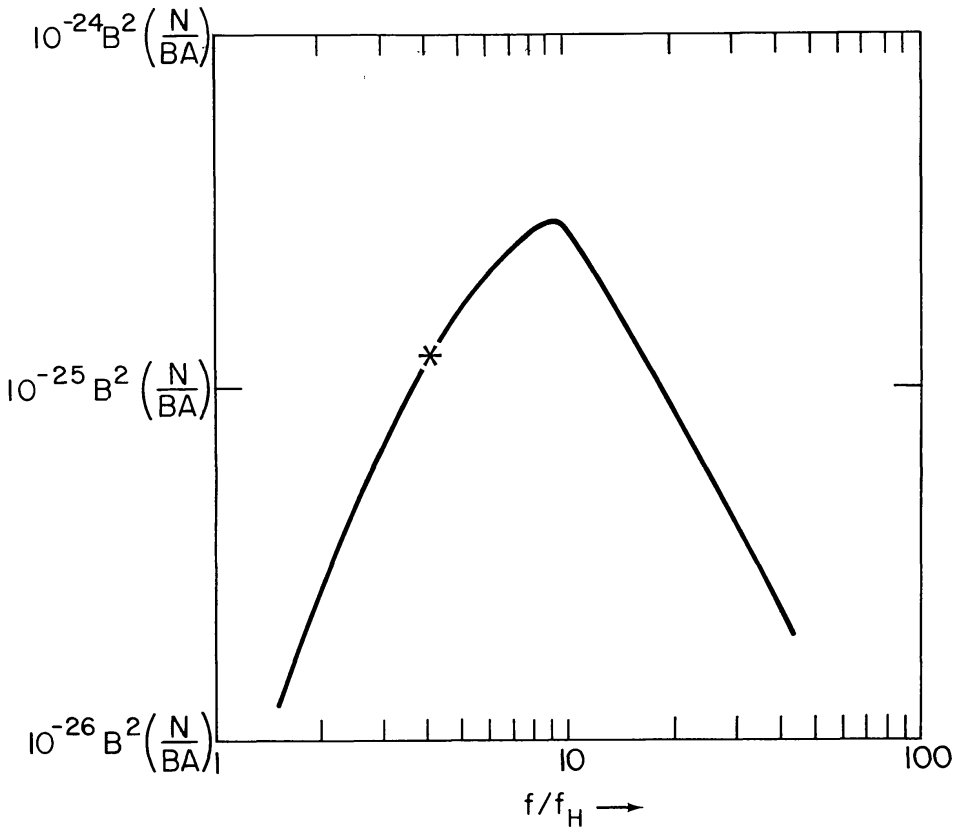

Fig. 21. Gyro-synchrotron intensity with effects of self-absorption and suppression by the ambient plasma, for $\Omega_e/\omega_e \sim 1$ where $N(\mathrm{cm}^{-3})$ is the total number of energetic electrons in the source, B is the strength of the magnetic field and $A(\mathrm{cm}^{-2})$ is area of the radiating volume (after Ramaty, 1973).

and Razin effect change the spectrum. In Table I, we also evaluate the turnover frequency $f_{\max}$ given by Equations (21), (23), (24), and (25) for different parameters in the radiating source.

We conclude from Table I that for $\omega_e \leq \Omega_e$ the dominant absorption process is the thermal gyro-resonance absorption and $f_{\max} \sim 4f_H$. These are the results we have used freely without proof in Section 2. For $\omega_e > \Omega_e$, the free-free absorption and Razin effect are the dominating absorption processes. The spectra in this case are flat for $f < f_{\max}$ and are rarely observed (Hachenberg and Wallis, 1961). In the rest of this article we will

TABLE I

$L = 10^9$ cm, $T_e \simeq 10^7$ K, $I = 10$ sfu

Turnover frequency	$N = 10^9$ cm^{-3} $B = 400$ G $\omega_e < \Omega_e$	$N = 10^{10}$ cm^{-3} $B = 300$ G $\omega_e \simeq \Omega_e$	$N = 10^{11}$ cm^{-3} $B = 100$ G $\omega_e > \Omega_e$
$f^{th}_{\max}$	5 GHz	1 GHz	0.3 GHZ
$f^{r}_{\max}$	6×10^{-2} GHz	3×10^{-1} GHz	9 GHZ
$f^{ff}_{\max}$	7×10^{-2} GHz	7×10^{-1} GHz	7 GHz
$f^{sa}_{\max}$	59×10 GHz	5×10 GHz	10 GHz

consider them to be the exception and not the rule, so we will assume that $\omega_e \simeq \Omega_e$ in the microwave emitting region. One important point is the fact that self-absorption for frequencies $f < f_{\max}^{sa}$ will change the emitted mode e.g., for $f < f_{\max}^{sa}$ the source is optically thick and the ordinary mode dominate the emission, for $f > f_{\max}^{sa}$ the source is opticaly thin and most of the radiation is in the extraordinary mode. In Figure 21 we denote with an asterisk the frequency where the sense of polarization reverses. Several observations including the recent ones by Kundu *et al.* (1982a) have indicated this frequency reversal at $f = 5$ GHz for relatively strong bursts.

(iii) *Electromagnetic Radiation from Weakly Turbulent Plasmas*

We have argued several times in this article that microwave bursts are the signatures of the interaction between the energetic electrons released from the flare and the magnetic field surrounding the flaring region. One obvious question that can be asked then is the following: Are the streaming electrons stable against plasma instabilities? Is there enhanced emission with fine structures observed in the microwave domain that are related to these instabilities as at decimeter and meter wavelengths?

One can immediately argue that the radiation from several plasma instabilities even if they are excited in the low corona will not escape, especially from regions where $\omega_e < \Omega_e$ since, in the inner corona the gyro-thermal absorption, as discussed above, will absorb the radiation around Ω_e, $2\Omega_e$ and sometimes $3\Omega_e$. But as we will show in Section 4, under certain conditions the radiation from the nonlinear interaction of two upper hybrid waves excited from the streaming electrons (Vlahos *et al.*, 1981) or even plasma radiation at $2\omega_e$ for the relatively rare cases where $\omega_e > \Omega_e$ can escape.

Indeed, as we have discussed earlier the high time resolution observations (Slottje, 1978) show that fine time structure pulses with brightness temperatures as high as 10^{15} K exist. These pulses are probably the signatures of plasma instabilities in the low corona (Holman *et al.*, 1979; Kuijpers *et al.*, 1981; Vlahos *et al.*, 1982).

(iv) *Collisional Bremsstrahlung*

We close this subsection by reviewing the characteristic properties of the spectrum when the emission mechanism is dominated by the photons emitted at close encounters between thermal electrons and ions. The emission at frequencies $f < f_{\rm cr}$ increases as f^2 and remains constant above $f_{\rm cr}$, where $f_{\rm cr}$ is given by (Zheleznyakov, 1970)

$$f_{\rm cr}^2 = 2 \times 10^{-22} N^2 L [T(\mathrm{K})]^{-3/2} \tag{26}$$

and

$$I(f < f_{\rm cr}) = 0.5 T_6^{-1/2} f_9^2 N_{10}^2 L_9^3 \text{ sfu} . \tag{27}$$

The polarization in this case is less than a few percent. It has been known for many years that the spectrum slowly changes during the post burst phase of the flare. We believe that the old as well as the recent results (Kundu, 1959; Alissandrakis and Kundu, 1978) strongly suggest that in the post burst phase the collisional bremsstrahlung dominates the emission. This is in accordance with a simple picture of the evolution of energy release

in the flaring region, namely, the thermal and/or the energetic electrons released will heat the upper portions of the chromosphere which in turn will 'evaporate'. The fact that the density in the low corona will increase drastically in the post burst phase as indicated also from the enhancement of soft X-ray emission in this phase, and the decrease of the temperature as the size of the source increases favors the collisional bremsstrahlung (see Equation (27)) for this phase. But as we can easily prove collisional bremsstrahlung can be invoked only in rare situations as the emission mechanism for the impulsive phase.

3.3. Summary

We have discussed in this section several factors which play important roles in determining the shape of the spectrum of the power emitted and the polarization of centimeter bursts from a flaring region. We outline here the basic unknown parameters in modelling the radiating region.

(a) The volume of the emitting region, (b) the number of streaming electrons $N_s = \int f_s \, dv$, when a streaming population of electrons is involved, (c) the strength of the magnetic field B_s at the source and its scale $L_H = B_s \, (dl/dB)$, and (d) the density N and temperature T of the ambient thermal plasma.

The existing observations as outlined in Section 2, provide the following direct information.

The size of the burst source, its intensity and polarization at one or two wavelengths can be obtained from two dimensional maps, with time resolution of 10 s, spatial resolution of 1″ arc or better with the VLA or the WSRT. The spectra can be derived from simultaneous observations made at several frequencies at other observatories. A problem here is the difference in spatial resolution of different instruments which may cause difficulties since many independent sources may contribute to the emission observed by low resolution instruments and alter the shape of the spectrum. However in some selected isolated strong events with fluxes $I_m > 10$ sfu we can sometimes construct a reliable spectrum.

Finally simultaneous observations with arc sec resolution from the same region in soft X-rays or EUV and microwaves will be extremely useful to obtain estimates of the ambient density and temperature (N, T). Measuring the emission measure ε^* and effective line-of-sight temperature T^* by using two different wavelength bands we can solve for N (Kundu *et al.*, 1979).

Analyzing the information collected from the above observations we can easily extract several parameters of the emitting region. The shape of the spectrum combined with the information about N, T can give us information about the velocity distribution e.g., if the slope for $f > f_{\max}$ is much larger than 3–4, the velocity distribution for the energetic electrons is Maxwellian; on the other hand, for $f < f_{\max}$ if the spectrum is flat, then free-free absorption dominates, which in turn will contain information about the magnetic field strength. The turnover frequency, also gives us an estimate of the average magnetic field in the source (if $\omega_e < \Omega_e$).

In Section 4 we review different microwave burst models proposed over the past several years.

4. Microwave Burst Models

Microwave bursts provide one of the many signatures of the explosive energy release in the Sun's atmosphere, called a flare. Discussion of the properties of the flare emission over a wide range of wavelengths has been the subject of several recent books (Švestka, 1976; Sturrock *et al.*, 1980). A comprehensive solar flare model must be able to answer three fundamental questions: (a) what are the details of the mechanism(s) which convert magnetic energy to plasma kinetic energy and/or particle acceleration; (b) the physical processes involved in transporting energy from the energy release site to other regions of the solar atmosphere; and (c) the radiation processes responsible for the observed bursts at various wavelengths.

As discussed in Section 2, the statistical correlation of microwave and hard X-ray bursts is nearly 100%. The intensity peaks at both wavelengths are nearly coincident in time, within the limits of time resolution of the presently available measurements. This information has been extensively used in modelling the microwave and hard X-ray burst sources. In modelling a microwave source most authors have assumed that the two burst sources are cospatial.

We now review the existing models in the historical order as they have appeared in the literature. We emphasize two parts in each model: (a) How is it related to the overall flare model; (b) what are the suggested model parameters necessary to calculate the spectrum (e.g., the structure of the magnetic field, the shape of the velocity distribution etc.).

4.1. The Magnetic Trap Model

The magnetic trap model was initially suggested by Takakura and Kai (1966) and revised later by Takakura (1969, 1972). The basic idea in this model is the following: The bulk of the flare energy goes into accelerating the electrons and protons. The energetic electrons are contained in a magnetic trap. Near the foot points of the trap the nonthermal electrons produce microwave bursts via gyro-synchrotron radiation. At the same time they lose energy and are thermalized by Coulomb collisions with the ambient protons of the thermal plasma, radiating hard X-ray bursts. The ambient plasma in the low corona is heated up to 20–40 million degrees Kelvin. This hot plasma may be cooled down in a few minutes to 10^6 K due to conduction and radiation losses. Heat flow along the magnetic field lines from the upper part of the trap would heat the chromosphere and the photosphere to emit EUV, Hα and the white light flare, while the nonthermal electrons stream into the chromosphere in heating the upper part of the chromosphere. It is not clear if the model works in its entirety. Takakura (1972) elaborated only a part of this model, namely the interpretation of the microwave and hard X-ray bursts.

Using his model, Takakura calculated the spectrum and time evolution of the microwave burst emission. For the magnetic field geometry, he used a dipole field located at a depth $d = 10^4$ km under the photosphere, and the strength of the magnetic field at the photosphere was set at $B \simeq 2500$ G. The radio source has a lower boundary at the top of the chromosphere. The maximum value of the magnetic field $B(1)$ at the radio source,

assuming a dipole field is given by $B(1) = 0.47B(0)$. The upper boundary of the source is set at an equistrength surface of the magnetic field $B(2) \simeq 60$ G as in Figure 22. The upper boundary may be due to the upper boundary of the trapping region of the nonthermal electrons or an effective boundary due to the Razin effect which, as we mentioned earlier, suppresses the gyro-synchrotron radiation in weak magnetic fields (e.g., $\omega_e > \Omega_e$). The velocity distribution function in the radio source is assumed to be homogeneous, with an isotropic pitch angle distribution and a power law energy distribution with a change of the exponent Γ at 100 keV, that is

$$N(\varepsilon)\, d\varepsilon = G\varepsilon^{-\Gamma}, \tag{29}$$

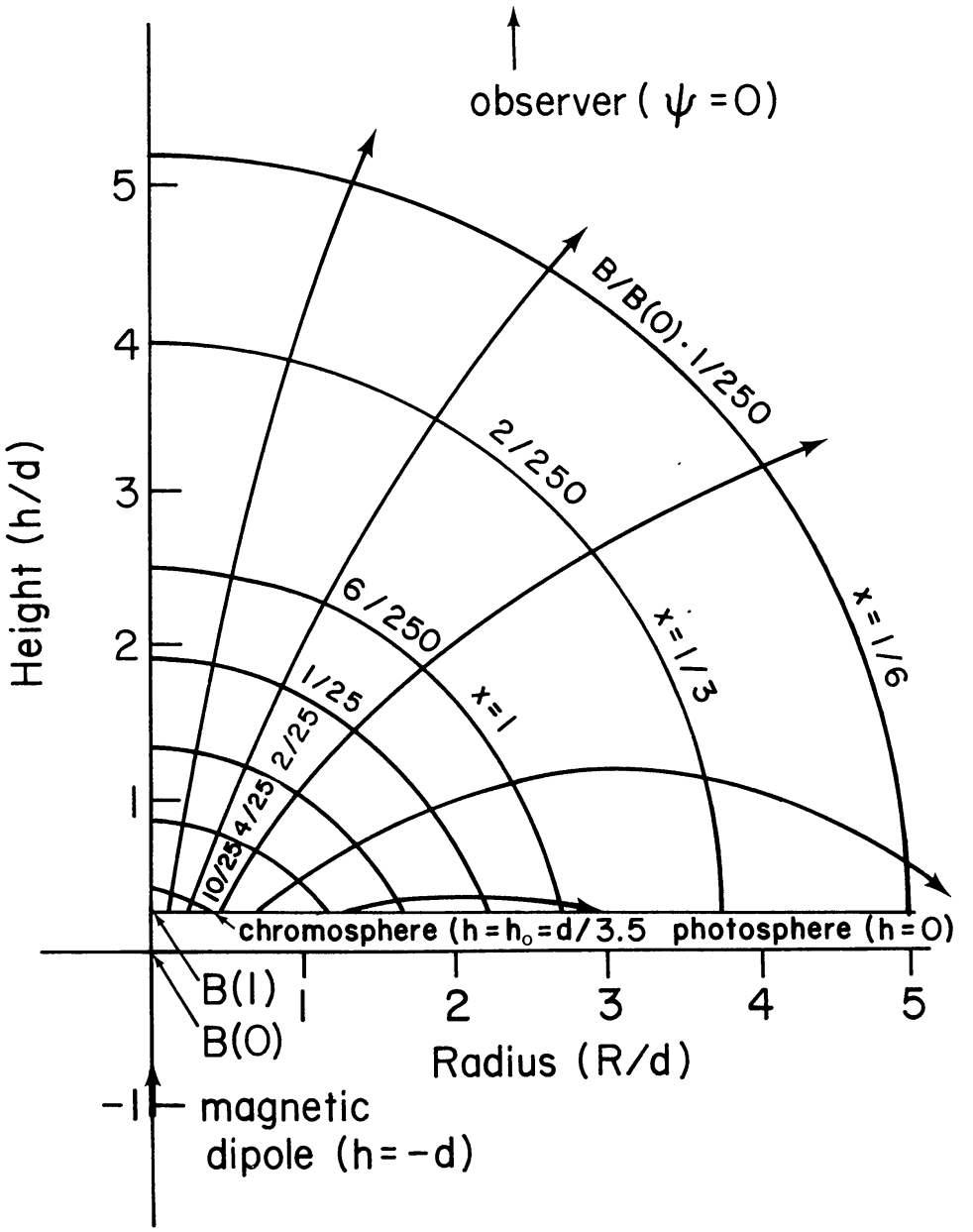

Fig. 22. Model of magnetic field in the radio source showing a cross section in the ecliptic plane. The radio source is axially symmetric about the axis of the magnetic dipole in a limited range of the azimuthal angle ϕ, X is a measure for the upper boundary of the radio source. The normalized value of the magnetic field strength is indicated on the curves (after Takahura, 1972).

where $G = G_0$ and $\Gamma = 4$ for $\varepsilon \geq 100$ keV, $G = 5G_0$ and $\Gamma = 3$ for 10 keV $< \varepsilon <$ 100 keV and $G = 0$ for $\varepsilon < 10$ keV. The thermal temperature of the ambient plasma inside and outside the microwave source is 10^7 K. The density of the thermal electrons is such that $\omega_e < \Omega_e$ everywhere in the source. Typical volumes used by Takakura in his computations were $\simeq 10^{29}$ cm^3 for the entire radio source at its peak emission ($L \sim 2'$ arc), which is at least 100 times larger than the average microwave source, as measured recently with large telescopes such as the VLA or the WSRT.

A major problem encountered by this model is that it is unable to explain the large discrepancy between the numbers of nonthermal electrons estimated from hard X-ray and from microwave burst emissions. X-ray estimates give about a thousand times more electrons of the same energy above 50 or 100 keV. Takakura (1972) claimed that by using a nonuniform magnetic field, a change in the slope (see Equation (29)) of the energy distribution and by including self-absorption in his calculations, he could solve this number discrepancy problem.

Another problem Takakura (1972) had overlooked was the question of stability of the streaming electrons with energy $\varepsilon > 20$ keV. Indeed, he used $N_s = \int f_s \, dv = N_e$ in his calculations. In such a case the electrons will relax quasilinearly to form a plateau in velocity space (see Vlahos and Papadopoulos, 1979).

The time evolution of the spectrum was also discussed by Takakura and Kai (1966), Takakura *et al.* (1969), and Takakura (1972). In order to account for the time variation of the microwave spectrum, we must take into account the time variation of the energy distribution of the energetic electrons $N_s(\varepsilon, t)$, the time variation of the emitting volume $V_s(t)$ and possibly also the magnetic field $\bar{B}(\bar{r}, t)$. Takakura and Kai (1966) assumed that acceleration ends off at the time of maximum intensity and $(dV_s/dt) = (dB/dt) = 0$. Thus the main factor in the spectral change in the decay phase is due to the energy changes of the trapped electrons. They have also assumed that energy is lost only through radiation and/or collisions.

The presently available VLA observations show clearly that the volume as well as $N_s(\varepsilon, t)$ change radically in the decay phase. It is thus important to update these calculations.

4.2. The two-component model

The two-component model was suggested by Böhme *et al.* (1977). This model is based on a phenomenological manifestation of the X-ray and microwave bursts. They suggested that a core-halo structure may exist during the impulsive phase of the flare. The flare energy is released in two forms: (a) it heats a large volume with $L > 10^9$ cm up to a temperature $T \sim 3 \times 10^7$ K and (b) it heats and accelerates electrons in a smaller core ($L \simeq 10^9$ cm) where the distribution is Maxwellian with temperature $T_e \sim 10^7$ up to a velocity V_c and a power law distribution above V_c. The density in the core is 10^{10} cm^{-3} but drops to 10^9 cm^{-3} in the halo. No attempt was made to relate such a structure to a specific flare model. Böhme *et al.* also assumed that the magnetic field changes slowly with height and has a maximum value of ~ 1500 G, in the lower part of the radiating region.

The estimated spectra, from the above model, are divided into three ranges: (a) for $f > 10$ GHz, the radiation originates in the core only; (b) for 10 GHz $> f > 5$ GHz, the radiation comes partly from the core and partly from the halo region and (c) for $f < 5$ GHz the radiation originates in the halo only (radiation from the core in this frequency range is reabsorbed in the halo). Their computed spectra have unreasonably high steepness at high frequencies, which is probably due to an artificial cut-off in velocities above a few hundred keV. They also assumed that the hard X-ray source coincided with the core and soft X-ray with the halo and estimated the X-ray emission from the same source.

The above model can have a practical value in some stage of the flare evolution e.g., if the core is identified with a compact loop and the halo with an overlying larger loop heated up to a few times 10^7 K during the impulsive phase. But these circumstances are not common and so the validity of their model is rather limited.

4.3. The thermal model

The thermal model was proposed by Matzler (1980) and Dulk *et al.* (1979) to explain the impulsive phase of hard X-ray and microwave bursts. They suggested that the bulk of the magnetic energy goes into heating and the plasma is heated to high temperatures, $T_e \simeq 2 \times 10^8$ K or higher. They used a Maxwellian velocity distribution to estimate the gyro-synchrotron radiation from a plasma with density of 10^9 cm^{-3}. Dulk *et al.* used a constant magnetic field strength of $\simeq 10^2$ G; Matzler, on the other hand, assumed that the magnetic field changed from 100 to 1000 G. Their calculations were motivated by the observations of Chubb (1966) and Crannel *et al.* (1978) in which the spectrum of a special class of hard X-ray bursts fit better to a Maxwellian distribution with one temperature. Further motivation for this kind of model came from the theoretical suggestions of Brown *et al.* (1979), which assumes that the magnetic energy is released in a small volume (energy release volume – ERV) compared to the volume of the loop, and the rate at which magnetic energy is transformed into plasma energy is faster than the energy losses from the same volume. This causes a local enhancement of the temperature by as much as two orders of magnitude above the coronal temperature. They also assumed that the bulk of the energy released goes into heating, which primarily heats the electrons ($T_e > T_i$). Using the above assumptions one can easily show (Brown *et al.*, 1979; Vlahos and Papadopoulos, 1979) that the high energy electrons in the tail of the velocity distribution in the impulsively heated region will instantaneously run away from this volume and the resulting charge imbalance between the ERV and its surrounding (which have average coronal temperature $\sim 10^6$ K) will drive a return current, with velocity V_D. When V_D reaches the value of the local sound speed $\sim 10^8$ cm s^{-1}, low frequency ion acoustic waves will be excited in the interface of the ERV and its surroundings. It has been shown that the heat flow along the magnetic field lines is greatly reduced due to the presence of ion-acoustic turbulence (cf., Manheimer, 1977) and this makes the above model a favorable candidate for hard X-ray source. Dulk *et al.* (1979) excluded the dynamic evolution of the escaping electrons assuming that the entire plasma is 'trapped' in ERV. As we will point out in the next section, inclusion of the dynamical

evolution of these electrons has an important effect on the microwave burst emission but changes little the argument about the 'thermal' interpretation of hard X-ray bursts, particularly those with low energy $E < 30$–40 keV.

4.4. Flaring loop model

The Flaring Loop Model (Vlahos and Papadopoulos, 1979; Emslie and Vlahos, 1980) is based upon the assumption that the active region is a collection of magnetic loops of different sizes and magnetic field strengths. It poses the following question: What will be the response of the plasma in one of the loops in the case that magnetic reconnections release energy locally at the top of the loop impulsively (≤ 1–2 s) at a rate faster than the dissipation losses (e.g., convection, conduction, radiation, etc.). It is also assumed that the energy released heats primarily the electrons ($\partial T_e/\partial t > \partial T_i/\partial t$) but at the same time *strong electric fields* develop along the magnetic field with a strength (Bateman, 1978; Van Hoven, 1979; Spicer, 1981)

$$E_z \simeq V_x^1 B_* + \eta J_z^1 , \tag{30}$$

where V_x^1 and B_* and J_z^1 are shown in Figure 23.

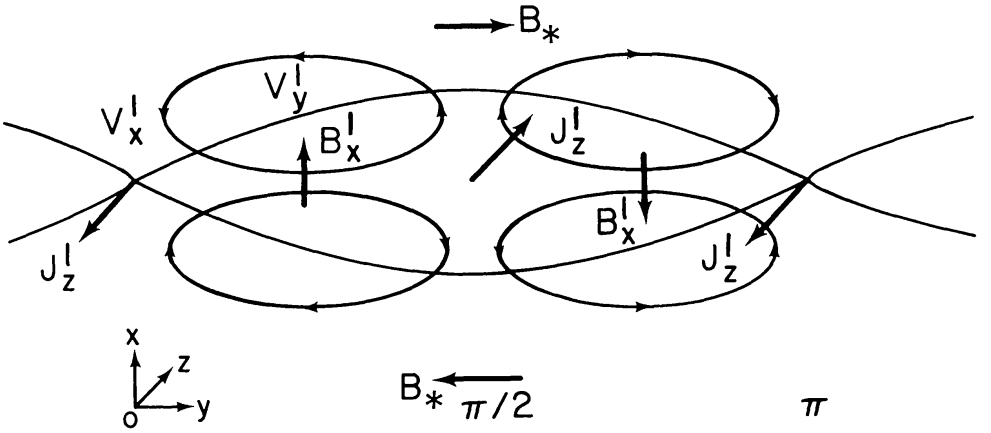

Fig. 23. The magnetic field, longitudinal current density, and flow pattern of a tearing mode are shown together with the separatrix of the induced magnetic island (Bateman, 1978).

According to the above model multiple bursts may sometimes be caused by the energization of several loops in the active region but for the sake of simplicity we shall consider only one loop in the rest of our discussion here and the generalization can easily follow.

We divide the Flaring Loop in three distinctive regions (see Figure 24). Region I is the region where the energy is released initially and it is related to the wavelength of the reconnecting mode. It can be anywhere in the loop as long as it occupies a small fraction of the loop volume. Region II is the region where the high energy electrons streaming out of region I are forming beam-like velocity distributions and finally region III is the region where the energetic electrons precipitate and thermalize due to collisional interactions with ions in the transition zone and upper chromosphere. The above division of the loop in three regions is meaningful only in the initial stages of the energy release (10–50 s

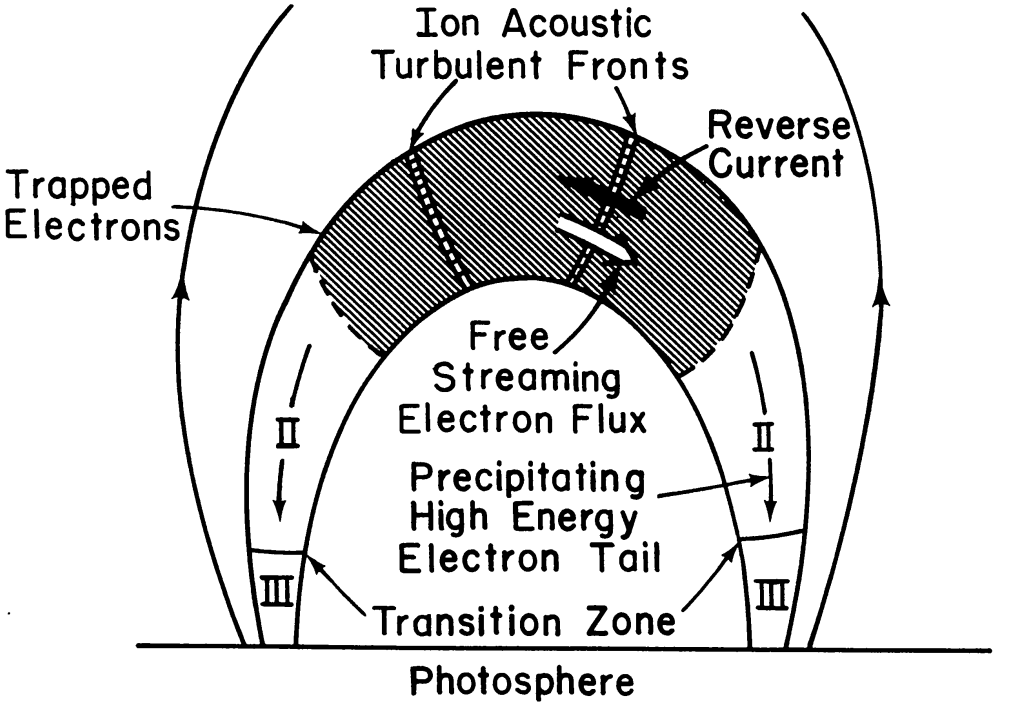

Fig. 24. Schematic of the flaring loop model (cf., Vlahos and Papadopoulos, 1979). In region I the energy release occurs by magnetic reconnection, causing hot electrons to stream into region II. The associated reverse current builds-up turbulent plasma fronts as shown: this restricts the free streaming of the hot electrons and sets-up a marginally stable state, with very energetic electrons ($V > V_c$) precipitating out of region I to partialy balance the reverse current. Region III represents the dense (chromospheric) region of the loop.

around the peak of the burst), since over time periods longer than 1 min, one must consider the expansion of regions I and III, which will alter the density and temperature in region II.

We can use several model velocity distributions for the electrons in region I. In our discussion here we assume that due to the presence of strong electric fields in region I, the tail of the distribution is freely accelerated and form a power law for $V > V_c$. We can uniquely determine V_c if we require that electrons with velocity $V > V_c$ will escape from region I without collisions. Collisions between electrons and ions in region I are unimportant due to the low density ($N = 10^{10}$ cm^{-3}) and high temperature in this region. On the other hand, the effective collision frequency between electrons and ion acoustic waves in the turbulent front existing in the boundary between region I and II give an upper limit for V_c determined from the equation (Vlahos and Papadopoulos, 1979).

$$\frac{V_c}{V_e} = \left(\frac{L_I}{\lambda_D}\right)^{2/5} (\omega_e t_0)^{-1/5} (\nu^x/\omega_e)^{1/5}, \tag{31}$$

where t_0 is the duration of the impulsive phase of the burst, L_I is the thickness of the shock and ν^x is the effective collision frequency which for a marginally stable condition (Papadopoulos, 1977) is approximately equal to $10^{-2}\omega_e$. For $L_I = 10^8$ cm, $\lambda_D = 1$ cm, $\omega_e \sim 10^9$ s^{-1} and $\tau_0 \simeq 10^2$ s, we find $V_c \simeq 3V_e$. Thus electrons with velocity $V > 3V_e$ stream along the magnetic field lines with energies $E > 100$ keV forming beams in

region II, while electrons with velocity $V < 3V_e$ will take times longer than the impulsive phase to 'escape' from region I. As we explained in the previous section the escaping electrons play an important role in the maintenance of the ion acoustic fronts since they will drive the return current. The minimum number of escaping electrons can be determined from the equation $N_b V_b \geq NC_s$ or

$$\frac{N_b}{N} > \frac{C_s}{V_b}. \tag{32}$$

The final question one has to answer before we end the discussion on the dynamic evolution of the streaming electrons is the question of stability against plasma waves excited by these electrons. The question of two-stream instability of the precipitating beams has been analyzed by Vlahos and Papadopoulos (1979). They showed that the beam will remain stable and lose very little energy to the waves in region II if

$$\frac{N_b}{N} \lesssim 10^{-4} [T_e^{\mathrm{I}}/T_e^{\mathrm{II}}]^2 \tag{33}$$

where T_e^{I}, T_e^{II} are the plasma temperatures in region I and II, respectively. Also since the electrons in the escaping tail are primarily accelerated along the magnetic field lines, they have a velocity distribution with $V_\parallel > V_\perp$ (the components respectively parallel and perpendicular to the magnetic field lines), and therefore the anomalous Doppler resonance instability is excited (e.g., Kadomtsev and Pogutse, 1969; Liu and Mok, 1977; Liu *et al.*, 1977). The growth rate γ is given by the equation

$$\gamma \simeq (N_b/N)\,(T_e^{\mathrm{I}}/T_e^{\mathrm{II}})^{1/2}\,\omega_e\,. \tag{34}$$

For $N_b/N \sim 10^{-2}$ and $T_e^{\mathrm{I}}/T_e^{\mathrm{II}} \sim 10^2$ we obtain $\gamma \sim 10^{-3}\,\omega_e \simeq 10^{-6}$ s. Thus the growth time of the electron cyclotron waves is very much shorter than the loop transit time of the electron i.e., the instability saturates well before the electron beam can reach the chromosphere. Since the anomalous Doppler resonance instability diffuses through pitch angle scattering, the high energy electrons in the tail change from a distribution in which $V_\parallel \gg V_\perp$ to one with $V_\parallel \sim V_\perp$ the number of trapped electrons in the loop will radically increase. Electrons will stay out of the precipitating (loss) cone only if

$$\frac{V_\parallel}{V_\perp} \lesssim \left(\frac{\delta B}{B}\right)^{1/2}, \tag{35}$$

where δB reflects the change in longitudinal magnetic field B within L^{II}. The number of trapped electrons is obtained by integrating the velocity distribution of streaming electrons between $(\omega_e + \Omega_e)/K_\parallel$ and V_M; we find that approximately 10% of the beam particles are trapped, so that $(N_H/N) \sim 10^{-3}$, where V_M is the maximum velocity in the distribution of the streaming electrons and N_H the number density of trapped electrons (Vlahos, 1979). The partial trapping of the escaping electrons solves in a natural way the outstanding problem between the differences in numbers required to produce hard X-ray and microwave bursts from the same population of electrons trapped in the same volume.

We mentioned in Section 2 that the high resolution VLA observations often suggest that the microwave emission originates from the upper part of a magnetic loop or arcade of loops (e.g., Marsh and Hurford, 1980; Kundu *et al.*, 1982a). Holman *et al.* (1982) have recently showed that this phenomenon is a direct consequence of the anomalous doppler resonance instability and the characteristic scale length of the magnetic field variation along the loop (L_H). If $L_H \ll$ length of the loop, a large fraction of the streaming electrons will be trapped in the upper part of the loop: if $L_H \simeq$ length of the loop, the trapping will be extended over larger volumes and the bipolar points will be further apart (in agreement with the observations of Kundu *et al.*, 1982a). Furthermore Holman *et al.* (1982) argue that since the trapped electrons will be only a fraction of the escaping electrons from the ERV the hard X-ray spectrum will show several breaks in high energies. Petrosian (1982) on the other hand examined the microwave intensity and spectrum due to gyro-synchrotron radiation from mildly relativistic electrons injected at the top of the loop and reached the conclusion that if (i) the magnetic field from the top to the footpoints of the loop does not increase very rapidly and (ii) the accelerated particles have a nearly isotropic pitch angle distribution then the microwave brightness will have a peak at the top of the loop. Thus we conclude that the isotropization of the initial field aligned velocity distribution of the energetic electrons due to anomalous doppler resonance not only increases the trapping, as discussed by Holman *et al.* (1982), but it will also increase the microwave brightness at the top as shown by Petrosian (1982).

It was pointed out by Holman *et al.* (1980) that the high brightness temperature microwave spikes observed by Slottje (1978) could result from gyrosynchrotron maser-ing. They noted that the loss cone distribution acquired by suprathermal electrons upon reflection in the legs of the flaring loop is unstable to the stimulated emission of gyrosynchrotron radiation. Melrose and Dulk (1982) have shown that amplification of the second harmonic of the gyrofrequency is sufficiently fast to account for the obser-vations. Sharma *et al.* (1982) have found, however, that the electron plasma frequency must be near the gyrofrequency so that saturation of the first harmonic does not prevent the growth of the second harmonic emission.

Vlahos *et al.* (1982) suggested recently that the intense fine time structure microwave bursts observed by Slottje (1978) can be explained by the flaring loop model as follows: the precipitating beam excites upper hybrid waves propagating in a direction opposite to the beam. They have shown that upper hybrid waves interact coherently if the amplitude of the interacting electrostatic waves is above a critical value (E_c). They showed that it is easy to explain the observed power if only 1% of the beaming electrons' energy goes to the waves. At the same time they found that the time structure observed is caused either from the fluctuation in the number of accelerated electrons or the depletion of the pump due to a change of the interaction mode (coherent or incoherent) efficiency around E_c.

Another important characteristic of the flaring loop model is that under several conditions discussed recently by Low (1981) a loop may lose its equilibrium and move slowly outwards (away from the Sun's surface). In this case the trapped electrons are carried with the loop causing a continuous change in the spectrum.

Once trapped, the electrons drift perpendicular to both $\overline{B}$ and $\overline{R}$ (outward curvature radius vector) with velocity

$$V_D = \frac{1/2 m_e c v_\perp^2}{BR} \simeq \frac{3 \times 10^{12}}{BR} \text{ cm s}^{-1} \tag{36}$$

and the number of particles drifting across the loop to open magnetic field lines is (Vlahos, 1980),

$$N_{\text{esc}} = \left(\frac{N_H}{N}\right) N 2\pi R (V_D \tau) L^{\text{II}} \simeq 10^{29} \text{ electrons} \tag{37}$$

for $(N_H/N) = 10^{-3}$, a loop field $B = 100$ G, $L^{\text{II}} \simeq 10^9$ cm and a corresponding source lifetime $\tau = L^{\text{II}}/c_s \simeq 10$ s.

Summarizing the above discussion the following qualitative aspects of the radiation signatures will be expected from the flaring loop model around the peak of the impulsive phase.

(i) *Hard X-ray* bursts with photon energy $\varepsilon \leq E_{\min}$ $(= \frac{1}{2} m v_c^2)$ are thermally produced within region I, while hard X-rays of all energies (e.g., $\varepsilon < E_{\min}$ and $\varepsilon > E_{\min}$) are emitted by thick target bremsstrahlung of the escaping high energy tail electrons upon interaction with the dense chromospheric layers (Emslie and Brown, 1980; Brown *et al.*, 1980).

(ii) *Microwave bursts* are produced primarily by gyro-synchrotron emission of the trapped electrons in region II of the loop (Vlahos and Papadopoulos, 1979; Emslie and Vlahos, 1980; Holman *et al.*, 1982; Petrosian, 1982).

(iii) The fine structure emission observed by Slottje (1978) can be explained as either gyrosynchrotron masering or as a signature of the nonlinear interaction of two upper hybrid waves, excited by the precipitating electrons (Vlahos *et al.*, 1982).

(iv) EUV and optical radiation will be produced when the precipating escaping high energy tail thermalizes in the chromosphere (Emslie and Vlahos, 1980) (region III).

(v) Energetic electrons will be injected into interplanetary space by cross-field drift and subsequent reflection back along open magnetic field lines (Vlahos, 1980).

The above model appears to be consistent with the observed fluxes and spectra in hard X-rays, microwaves, EUV and the interplanetary electrons (Emslie and Vlahos, 1980). The flaring loop model is based on a few basic assumptions about the form of the energy released in region I, and it does not belong to the simplistic classification of thermal or nonthermal models usually mentioned in the solar literature since it has elements from both models.

Kundu and Vlahos (1979) have used the above model to interpret the unipolar microwave bursts sometimes observed with high resolution instruments by assuming that magnetic loops can have asymmetric field strengths at the two footpoints. In this case the electrons are reflected at one footpoint and precipitate at the other.

The post burst evolution in the flaring loop model is far from straight forward but can be described qualitatively. The maximum time the energetic electrons remain trapped is given by the collisional deflection time

$$\tau_D = 2 \times 10^8 E^{3/2} (\text{keV}) N^{-1} \text{ sec} \tag{38}$$

which is 20 s for $E = 100$ keV and $N = 10^{10}$ cm^{-3}. On the other hand the hot plasma in region I and III slowly expands and fills the entire loop. The density and temperature in the post-flare loop will be radically different from the initial values. In this final stage a thermal model may be appropriate to describe the emitted radiation. Kundu (1959) and Kundu and Vlahos (1979) have suggested that in this phase the emission mechanism may be collisional bremsstrahlung, since the observed polarization is less than 5%.

An interesting question which has not been discussed theoretically is the cooling time of the post burst phase as it is observed simultaneously from spatially resolved microwave and soft X-ray features. Answering this question both observationally and theoretically will be of great importance for the understanding of the post-flare evolution of the plasma in the loop.

4.5. Summary

It is clear from our discussion of the models presented above that our understanding of the energy release process has changed step by step over the years. For example, Takakura (1973) postulated that nearly 100% of the energy released in a flare went into accelerating energetic electrons, while Mätzler (1978) and Dulk *et al.* (1979) postulated that 100% went into heating. The flaring loop model has elements from both models. The microwave models have been influenced by the development of our understanding of the physics of the energy release process in a flare and the observations of magnetic field structures in the flaring region.

We believe that all of the above models have certain values in different stages in the evolution of a burst. For example the flaring loop model is a viable interpretation of the microwave burst only for 10–50 s around the peak in intensity. For time $t >$ 1–2 min a thermal model may describe the results better, whereas in cases when two loops with different sizes are energized a core-halo geometry is possible (for example, the two loops can be located one above the other, the large loop can be in its post-flare stage while the small compact loop is just energized). Thus we conclude that the time resolution is very crucial in microwave burst observations, since the distribution of electrons changes considerably with time.

5. Discussion and Conclusions

In this review we have attempted to summarize the observational and theoretical results obtained over the past several years. Microwave burst emission is one of the many radiations that are emitted during the flare explosion. In the past, theoreticians have overlooked the importance of microwave bursts in constructing flare models due to the fact that microwave emission is a complex function of many parameters which are important but difficult to measure e.g., magnetic field strength, energy distribution of the radiating electrons, plasma parameters etc. Also arguments have been made that energy-wise the microwave bursts like radio bursts in general, carry only a small fraction of the total energy released in solar flares.

The observations and interpretations of microwave bursts presented in this review article have provided convincing evidence that the study of microwave bursts can provide new insights into the flare process. Of special importance are the high spatial resolution ($\lesssim 1''$ arc) observations which, combined with the progress made in plasma physics have provided much improved understanding of how the preflare energy is stored in coronal levels and then released via magnetic reconnections, how the impulsive energy release is preceeded by colliding loops forming neutral sheets either by the emergence of new magnetic flux with pre-existing loop or by the formation of two bipolar loops with opposite polarities or a quadrupole structure. The high resolution observations have also shown that the radio emitting electrons occupy a significant portion of both sides of a loop or an arcade of loops, including the top of the loop(s); this confinement appears to be accounted for by doppler resonance instability and characteristic scale length of magnetic field variation along the loop. The demonstration by the high time resolution (10–100 ms) observations of the existence of fine time structure in microwave burst profiles is an important result in flare physics. It implies the existence of component burst sources having brightness temperatures as high as 10^{15} K, which requires the coherent interaction of upper hybrid waves excited by precipitating electron beams in the flaring loop.

The high spatial resolution observations combined with theoretical interpretations clearly show that flare energy is released in at least two different ways, namely, in isolated loops and colliding loops forming neutral sheets. The results so far obtained have been rather qualitative. Much theoretical work will be needed to understand quantitatively the diverse microwave radiation signatures that are observed in flares.

Acknowledgements

We thank Drs C. Alissandrakis, E. Schmahl, and Gordon Holman for comments on the manuscript. This work was supported by NSF grant ATM–8103089, NASA grant 21–002–199 and NASA grant NAG W–81.

References

Alissandrakis, C. E. and Kundu, M. R.: 1975, *Solar Phys.* **41**, 119.
Alissandrakis, C. E. and Kundu, M. R.: 1978, *Astrophys. J.* **222**, 342.
Bateman, G.: 1978, *MHD Instabilities,* MIT Press, Cambridge, Mass.
Bekefi, G.: 1966, *Radiation Processes in Plasmas,* J. Wiley and Sons, Inc., N.Y.
Bohme, A., Fürstenberg, R., Hildebrandt, J., Saal, O., Krüger, A., Hoyng, P., and Stevens, G. A.: 1977, *Solar Phys.* **53**, 139.
Brown, J. C., Melrose, D. B., and Spicer, D. S.: 1979, *Astrophys. J.* **228**, 592.
Brown, J. C., Craig, I. J. B., and Karpen, J. T.: 1980, *Solar Phys.* **67**, 143.
Chubb, T. A., Kreplin, R. W., and Friedman, H.: 1966, *J. Geophys. Res.* **71**, 3611.
Cohen, M. H.: 1961, *Astrophys. J.* **133**, 978.
Crannell, C. J., Frost, K. J., Mätzler, C., Ohki, K., and Saba, J. L.:1978, *Astrophys. J.* **223**, 620.
Datlowe, D. N., Elcan, M. J., and Hudson, H. S.: 1974, *Solar Phys.* **39**, 155.
De Jager, C. and Kundu, M. R.: 1963, in W. Friester (ed.), *Space Research,* III, North-Holland Publishing Co., Amsterdam, Holland, p. 836.

Drake, J. F.: 1971, *Solar Phys.* **16**, 152.
Drummond, W. E. and Rosenbluth, M. N.: 1960, *Phys. Fluid* **3**, 45.
Dulk, G. A., Melrose, D. B., and White, S. M.: 1979, *Astrophys. J.* **234**, 1137.
Enome, S., Kakinuma, T., and Tanaka, H.: 1969, *Solar Phys.* **6**, 428.
Emslie, A. G. and Brown, J. C.: 1980, *Astrophys. J.* **237**, 1015.
Emslie, A. G. and Vlahos, L.: 1980, *Astrophys. J.* **242**, 359.
Felli, M., Tofani, G., Fürst, E., and Hirth, W.: 1975, *Solar Phys.* **42**, 377.
Frost, K. J.: 1969, *Astrophys. J. Letters* **158**, L159.
Fürst, E.: 1971, *Solar Phys.* **18**, 84.
Ginzburg, V. L. and Syrovatskii, S. I.: 1965, *Ann. Rev. Astron. Astrophys.* **3**, 297.
Gribbens, A. H. and Matthews, P. A.: 1969, *Nature* **222**, 158.
Guidice, D. A. and Castelli, J. P.: 1975, *Solar Phys.* **44**, 155.
Hachenberg, O. and Wallis, G.: 1961, *Z. Astrophys.* **52**, 42.
Heyvaerts, J., Priest, E. R., and Rust, D. M.: 1977, *Astrophys. J.* **216**, 123.
Hobbs, R. W., Jordan, S. D., Webster, W. J., Jr., Maran, S. P., and Caulk, H. M.: 1974, *Solar Phys.* **36**, 369.
Holman, G. D., Eichler, D., and Kundu, M. R.: 1980, in M. R. Kundu and T. E. Gergely (eds.), 'Radio Physics of the Sun', *IAU Symp.* **86**, 457.
Holman, G. D., Kundu, M. R., and Papadopoulos, K.: 1982, *Astrophys. J.*, (in press).
Hudson, H. S.: 1973, in R. Ramaty and R. G. Stone (eds.), *High Energy Phenomena on the Sun*, NASA SP-342, p. 257.
Janssens, T. J. and White, K. P.: 1970, *Solar Phys.* **11**, 299.
Janssens, T. J., White, K. P., and Broussard, R. M.: 1973, *Solar Phys.* **31**, 207.
Kadomtsev, B. B. and Pogutse, D. P.: 1968, *Soviet. Phys. JEPT.* **26**, 1146.
Kahler, S. W., Krieger, A. S., and Vaiana, G. S.: 1975, *Astrophys. J.* **199**, L57.
Kane, S. R.: 1972, *Solar Phys.* **27**, 174.
Karpen, J. T.: 1980, Ph.D. dissertation, University of Maryland, and NASA Report 82013.
Kattenberg, A.: 1981, Ph.D. dissertation, University of Utrecht, Netherlands.
Kaufman, P.: 1968, *Solar Phys.* **60**, 367.
Kuijpers, J.: 1974, *Solar Phys.* **36**, 157.
Kuijpers, J., Peter von de Post, and Slottje, C.: 1982, *Astron. Astrophys.*, (in press).
Kundu, M. R.: 1959, *Ann. Astrophys.* **22**, 1.
Kundu, M. R.: 1961, *J. Geophys. Res.* **60**, 4308.
Kundu, M. R.: 1963, *Space Sci. Rev.* **2**, 438.
Kundu, M. R.: 1965, *Solar Radio Astronomy*, Interscience, N.Y.
Kundu, M. R.: 1980, in M. R. Kundu and T. E. Gergely (eds.), *Radio Physics of the Sun*, D. Reidel Publ. Co., p. 157.
Kundu, M. R.: 1981, 'Solar Maximum Year', (*Proceedings International Workshop*, Simferopol, March 1981), *IZMIRAN Moscow* **1**, 24.
Kundu, M. R. and Alissandrakis, C. E.: 1975, *Nature* **257**, 465.
Kundu, M. R. and Haddock, F. T.: 1960, *Nature* **186**, 610.
Kundu, M. R. and Spencer, C. L.: 1963, *Astrophys. J.* **137**, 572.
Kundu, M. R. and Vlahos, L.: 1979, *Astrophys. J.* **232**, 595.
Kundu, M. R., Velusamy, T., and Becker, R. H.: 1974a, *Solar Phys.* **34**, 217.
Kundu, M. R., Becker, R. H., and Velusamy, T.: 1974b, *Solar Phys.* **34**, 185.
Kundu, M. R., Alissandrakis, C. E., and Kahler, S. W.: 1976, *Solar Phys.* **50**, 429.
Kundu, M. R., Alissandrakis, C. E., Bregman, J. D., and Hin, A. C.: 1977, *Astrophys. J.* **213**, 278.
Kundu, M. R., Schmahl, E. J., and Gerassimenko, M.: 1979, *Astron. Astrophys.* **82**, 265.
Kundu, M. R., Bobrowsky, M., and Velusamy, T.: 1981, *Astrophys. J.* **251**, 342.
Kundu, M. R., Schmahl, E., and Velusamy, T.: 1982a, *Astrophys. J.* **253**, 963.
Kundu, M. R., Schmahl, E., Velusamy, T., and Vlahos, L.: 1982b, *Astron. Astrophys.* **108**, 188.
Lacy, C. H., Moffet, T. J., and Evans, D. S.: 1976, *Astrophys. J. Suppl.* **30**, 85.
Lang, K. R.: 1974, *Solar Phys.* **36**, 351.
Lang, K. R.: 1977, *Solar Phys.* **52**, 63.
Liu, C. S. and Mok, Y. C.: 1977, *Phys. Rev. Letters* **38**, 162.
Liu, C. S., Mok, Y. C., Papadopoulos, K., Englemann, F., and Barmatici, M.: 1977, *Phys. Rev. Letters* **59**, 701.

Lewin, W. H. G. *et al.*: 1976, *Astrophys. J. Letters* **207**, L95.
Low, B. C.: 1981, *Astrophys. J.* **251**, 352.
Manheimer, W. M.: 1977, *Phys. Fluids* **20**, 265.
Marsh, K. A. and Hurford, G. J.: 1980, *Astrophys. J. Letters* **240**, L111.
Marsh, K. A., Zirin, H., and Hurford, G. J.: 1979, *Astrophys. J.* **228**, 610.
Marsh, K. A., Hurford, G. J., and Zirin, H.: 1980, in M. R. Kundu and T. E. Gergely (eds.), 'Radiophysics of the Sun', *IAU Symp.* **86**, 191.
Mätzler, C.: 1978, *Astron. Astrophys.* **70**, 181.
Melrose, D. B. and Dulk, G. A.: 1982, *Astrophys. J.* (submitted).
Pallavicini, R. and Vaiana, G. S.: 1976, *Solar Phys.* **49**, 297.
Papadopoulos, K.: 1977, *Rev. Geophys. Res.* **15**, 173.
Parker, E. N.: 1977, *Ann. Rev. Astron. Astrophys.* **15**, 45.
Parks, G. K. and Winkler, J. R.: 1966, *Solar Phys.* **16**, 186.
Petrosian, V.: 1982, *Astrophys. J. Letters,* in press.
Ramaty, R.: 1969, *Astrophys. J.* **158**, 753.
Ramaty, R.: 1973, in R. Ramaty and R. G. Stone (eds.), *High Energy Phenomena on the Sun*, NASA SP-342.
Ramaty, R. and Petrosian, V.: 1972, *Astrophys. J.* **178**, 241.
Rosenberg, H.: 1971, in R. Howard (ed.), 'Solar Magnetic Fields', *IAU Symp.* **43**, 652.
Rosner, R. and Vaiana, G. S.: 1978, *Astrophys. J.* **222**, 1104.
Rust, D. M.: 1977, in C. F. Kennel, L. J. Lanzerotti, and E. N. Parker (eds.), *Solar System Plasma Physics*, North-Holland Publ. Co., p. 51.
Sharma, R. R., Vlahos, L., and Papadopoulos, K. A.: 1982, *Astron. Astrophys.* (in press).
Sheeley, N. R. *et al.*: 1975, *Solar Phys.* **45**, 377.
Slottje, C.: 1978, *Nature* **257**, 250.
Smerd, S. F.: 1950, *Australian J. Sci. Res.* **43**, 34.
Somov, B.: 1979, *Solar Phys.* **60**, 315.
Spangler, S. R. and Shawhan, S. D.: 1974, *Solar Phys.* **37**, 189.
Spicer, D. S.: 1981, *Solar Phys.* **71**, 115.
Stenflo, J. O.: 1973, *Solar Phys.* **32**, 41.
Sturrock, P. A. (ed.): 1980, *Solar Flares – A Monograph from Skylab Solar Workshop II*, Boulder, University of Colorado Press.
Švestka, Z.: 1976, *Solar Flares,* D. Reidel Publ. Co., Dordrecht, Holland.
Tanaka, H.: 1961, *Proc. Res. Inst. Atmosph. Nagoya. Univ. Japan* **8**, 51.
Takakura, T.: 1962, *J. Phys. Soc. Japan*, Suppl. A-II, **17**, 243.
Takakura, T.: 1969, *Solar Phys.* **6**, 133.
Takakura, T.: 1972, *Solar Phys.* **26**, 151.
Takakura, T.: 1973, in R. Ramaty and R. G. Stone (eds.), *High Energy Phenomena on the Sun*, NASA SP-342, 179.
Takakura, T. and Kai, K.: 1966, *Publ. Astron. Soc. Japan* **18**, 57.
Tanaka, H. and Kakinuma, T.: 1962, *J. Phys. Soc. Japan,* Suppl. A-II, **17**, 211.
Turbnikov, B. V.: 1958, *Soviet Phys. Dokl.* **3**, 136.
Van Hoven, G.: 1979, *Astrophys. J.* **232**, 572.
Velusamy, T. and Kundu, M. R.: 1982, *Astrophys. J.* (July 15).
Vlahos, L.: 1979, Ph.D. Dissertation, University of Maryland, College Park.
Vlahos, L.: 1980, in M. R. Kundu and T. E. Gergely (eds.), 'Radio Physics of the Sun', *IAU Symp.* **86**, 173.
Vlahos, L. and Papadopoulos, K.: 1979, *Astrophys. J.* **233**, 717.
Vlahos, L., Sharma, R. R., and Papapdopoulos, K.: 1982, University of Maryland, preprint, AP82–010.
Vorpahl, J. A., Gibson, E. G., Landecker, P. B., McKenzie, D. L., and Underwood, J. H.: 1975, *Solar Phys.* **45**, 199.
Young, C. W., Spencer, C. L., Moreton, G. E., and Roberts, J. A.: 1961, *Astrophys. J.* **133**, 243.
Zheleznyakov, V. V.: 1970, *Radio Emission of the Sun and Planets,* Pergamon Press.